Parametric and Experimentally Informed BWR Severe Accident Analysis Using FeCrAl (M3FT-17OR020205041)

Nuclear Technology
Research and Development

Prepared for
U.S. Department of Energy
Advanced Fuel Campaign
Kevin R. Robb
Michael Howell
Larry J. Ott
Oak Ridge National Laboratory
August 2017
M3FT-17OR020205041
ORNL/SPR-2017/373

Nuclear Technology Research and Development–Advanced Fuels Campaign

Parametric and Experimentally Informed BWR Severe Accident Analysis Using FeCrAl (M3FT-17OR020205041)

Kevin R. Robb
Michael Howell
Larry J. Ott

Date Published:
August 2017

CONTENTS

LIST OF FIGURES

Page

LIST OF TABLES

ACRONYMS AND ABBREVIATIONS

ac	alternating current
ATF	accident-tolerant fuel
BWR	boiling water reactor
dc	direct current
DOE	US Department of Energy
FeCrAl	iron-chromium-aluminum alloy
HPCI	high-pressure coolant injection (system)
HTF	high-temperature furnace
KIT	Karlsruhe Institute of Technology
LTSBO	long-term station blackout
MSTSBO	mitigated short-term station blackout
ORNL	Oak Ridge National Laboratory
PMSBO	partially mitigated station blackout
RCIC	reactor core isolation cooling (system)
RMSD	root mean square deviation
RPV	reactor pressure vessel
SBO	station blackout
SRV	safety relief valve
STSBO	short-term station blackout

ACKNOWLEDGMENTS

ABSTRACT

Iron-chromium-aluminum (FeCrAl) alloys are being considered as advanced fuel cladding concepts with enhanced accident tolerance. At high temperatures, FeCrAl alloys have slower oxidation kinetics and higher strength compared with zirconium-based alloys. FeCrAl could be used for fuel cladding and spacer or mixing vane grids in light water reactors and/or as channel box material in boiling water reactors (BWRs). There is a need to assess the potential gains afforded by the FeCrAl accident-tolerant-fuel (ATF) concept over the existing zirconium-based materials employed today.

To accurately assess the response of FeCrAl alloys under severe accident conditions, a number of FeCrAl properties and characteristics are required. These include thermophysical properties as well as burst characteristics, oxidation kinetics, possible eutectic interactions, and failure temperatures. These properties can vary among different FeCrAl alloys.

Oak Ridge National Laboratory has pursued refined values for the oxidation kinetics of the B136Y FeCrAl alloy (Fe-13Cr-6Al wt %). This investigation included oxidation tests with varying heating rates and end-point temperatures in a steam environment. The rate constant for the low-temperature oxidation kinetics was found to be higher than that for the commercial APMT FeCrAl alloy (Fe-21Cr-5Al-3Mo wt %). Compared with APMT, a 5 times higher rate constant best predicted the entire dataset (root mean square deviation). Based on tests following heating rates comparable with those the cladding would experience during a station blackout, the transition to higher oxidation kinetics occurs at approximately 1,500°C.

A parametric study varying the low-temperature FeCrAl oxidation kinetics was conducted for a BWR plant using FeCrAl fuel cladding and channel boxes using the MELCOR code. A range of station blackout severe accident scenarios were simulated for a BWR/4 reactor with Mark I containment. Increasing the FeCrAl low-temperature oxidation rate constant (3 times and 10 times that of the rate constant for APMT) had a negligible impact on the early stages of the accident and minor impacts on the accident progression after the first relocation of the fuel. At temperatures below 1,500°C, increasing the rate constant for APMT by a factor of 10 still resulted in only minor FeCrAl oxidation.

In general, the gains afforded by the FeCrAl enhanced ATF concept with respect to accident sequence timing and combustible gas generation are consistent with previous efforts. Compared with the traditional Zircaloy-based cladding and channel box system, the FeCrAl concept could provide a few extra hours of time for operators to take mitigating actions and/or for evacuations to take place. A coolable core geometry is retained longer, enhancing the ability to stabilize an accident. For example, a station blackout was simulated in which cooling water injection was lost 36 hours after shutdown. The timing to first fuel relocation was delayed by approximately 5 h for the FeCrAl ATF concept compared with that of the traditional Zircaloy-based cladding and channel box system.

1. INTRODUCTION

The US Department of Energy (DOE) Fuel Cycle Research and Development Advanced Fuels Campaign is leading the research, development, and demonstration of nuclear fuels with enhanced accident tolerance [1]. Accident-tolerant fuels (ATFs) are fuels and/or cladding that, in comparison with the standard urania fuel–Zr-based alloy cladding system, can tolerate loss of active cooling in the core for a considerably longer time period while maintaining or improving the fuel performance during normal operations. Note that currently used urania–Zr-based cladding fuel systems tolerate design-basis accidents (and anticipated operational occurrences and normal operation) as prescribed by the US Nuclear Regulatory Commission. There are three major potential approaches for the development of ATFs

1. improving fuel properties,
2. improving cladding properties to maintain core coolability and retain fission products, and
3. reducing the rate of reaction kinetics with steam to minimize enthalpy input and hydrogen generation.

A proposed ATF concept is based on iron-chromium-aluminum alloys (FeCrAl) [2]. With respect to enhancing accident tolerance, FeCrAl alloys have substantially slower oxidation kinetics compared with currently used zirconium alloys. During a severe accident, FeCrAl would tend to generate heat and hydrogen from oxidation at a slower rate compared with zirconium-based alloys.

This report documents an extension of previous efforts to advance the development and assessment of the FeCrAl ATF concept. Oxidation tests with the B136Y alloy were conducted at Oak Ridge National Laboratory (ORNL) using simulated QUENCH test conditions. The simulated conditions (Section 2.2) were designed to aid in planning and in pre- and posttest calculations for an upcoming QUENCH test at the Karlsruhe Institute of Technology (KIT) that will also use the B136Y alloy. An additional series of oxidation tests using the B136Y alloy were conducted at ORNL following temperature ramp rates based on previous station blackout simulations (Section 2.3). These tests provide insight into the cladding behavior during anticipated accident conditions. Using the test data, the oxidation kinetics (Section 2.4), and the temperature at which rapid attack of the cladding by steam is initiated (Section 2.5) are examined. Insight from the tests is reflected in a parametric study of station blackout MELCOR simulations. Section 3 describes the accident scenarios chosen, figures of merit used in the comparison, MELCOR code, plant model, and modeling of FeCrAl in MELCOR. Section 4 provides the results of the accident simulations, and findings and suggested future work are discussed in Section 5.

2. EXPERIMENTAL WORK SUPPORTING QUENCH TESTING AND ACCIDENT ANALYSES

2.1 INTRODUCTION

The APMT FeCrAl alloy (Fe-21Cr-5Al-3Mo wt %) is a commercial alloy for which oxidation tests and the development of oxidation kinetics have been previously conducted [3]. However, development has been under way at ORNL to produce a material with properties suitable for nuclear reactor operations. For this application, the FeCrAl alloy Fe-13Cr-6Al (B136Y) is a first-generation alloy tested at ORNL that has more favorable irradiation properties than that of the commercial APMT alloy. B136Y will be used in a planned QUENCH test at KIT. Two series of oxidation tests in steam were performed with B136Y and are discussed in Sections 2.2 and 2.3. This is followed by a review of the test data with respect to oxidation kinetics (Section 2.4) and the onset temperature for rapid attack of the alloy by steam (Section 2.5).

2.1.1 Common Test Procedures

For both oxidation test series, tube segments of B136Y were exposed to a steam environment in ORNL's high-temperature furnace (HTF) [4]. Samples of B136Y tubing were taken from the same lot of tubing that will be used in the planned QUENCH test at KIT. The samples were approximately 9.51 mm OD and 12.62 mm long (see Appendix A for detailed measurements).

During the test, a cladding segment was first ramped from room temperature to 600°C under an argon atmosphere at a rate of 20°C/min. The sample was held at 600°C for one min. Following this test segment, the argon supply was shut off, steam was supplied to the test section, and the temperature was ramped at prescribed rates. Steam was supplied to the test section by injecting water into the lower portion of the preheat furnace at a constant rate of 0.0556 g/s (200 mL/h). The area averaged steam velocity, based on the geometry of the furnace, is provided in Table 1. The tests were concluded by turning off power to the furnace, turning off the steam supply, and supplying argon to the test section. All tests were performed at atmospheric pressure. Note that the measured, controlled, and reported temperatures are based on furnace thermocouples and are not measurements of actual sample temperatures.

Table 1. Steam velocity vs. temperature in the HTF

Temp. (°C)	Steam velocity(cm/s)
1,500	56.7
1,400	53.5
1,300	50.3
1,200	47.1
1,100	43.9
1,000	40.7
900	37.5
800	34.3
700	31.1
600	27.9

2.2   QUENCH-STYLE OXIDATION TEST SERIES

The first series of tests were conducted to aid in planning the future FeCrAl QUENCH test, provide insight into the anticipated behavior of the cladding during the QUENCH test, and help refine the oxidation kinetics for pre- and post-QUENCH test simulations.

2.2.1   Test Procedure

Within the capabilities of the HTF, samples were exposed to conditions (i.e., temperature vs. time with flowing steam environment) approximating those of the QUENCH-15 test (i.e., same as those planned for the FeCrAl QUENCH test). The various test segments are described in Table 2 and illustrated in Figure 1. Several tests were performed with various stopping points. The tests and temperature at which the tests were stopped are illustrated in Figure 2 and summarized in Table 3. Also included in Figure 1 and Figure 2 is data from the QUENCH-15 test for the 950 mm elevation (digitized from Fig. 19, red curve, Ref. [5]). Additional test details are provided in Appendix A. A unique test, 18, was conducted that extended the hold time of segment 2 to 150.9 min. This was conducted to investigate the effect of the "pre-oxidation" phase of the QUENCH tests on the FeCrAl alloy.

Table 2. Test segments: QUENCH-style oxidation tests

Segment	Ramp rate (°C/min)	Target temp. (°C)	Hold time at target temp. (min)
1	20	600	1
2	12	1,200	50.3
3	11.1	1,400–1,500	1
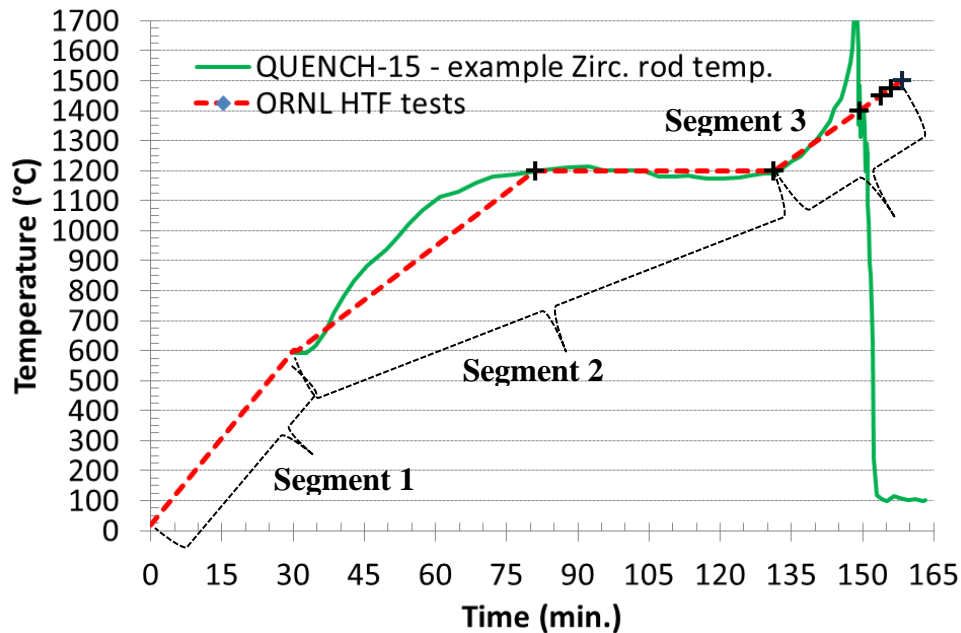
Figure 1. Heating segment illustration for QUENCH-style oxidation tests.

Table 3. Test number and maximum furnace temperature—QUENCH-style oxidation tests

Test	Maximum furnace temp. (°C)	Notes
1	1,200	Only 1 min hold after reaching 1,200°C
2	1,200	
3	1,400	
19	1,400	Repeat of test 3
15	1,450	
16	1,475	
4	1,500	
18	1,200	Similar to test 2; however, the hold time at 1,200°C was 150.9 min (3 times the duration of other tests).
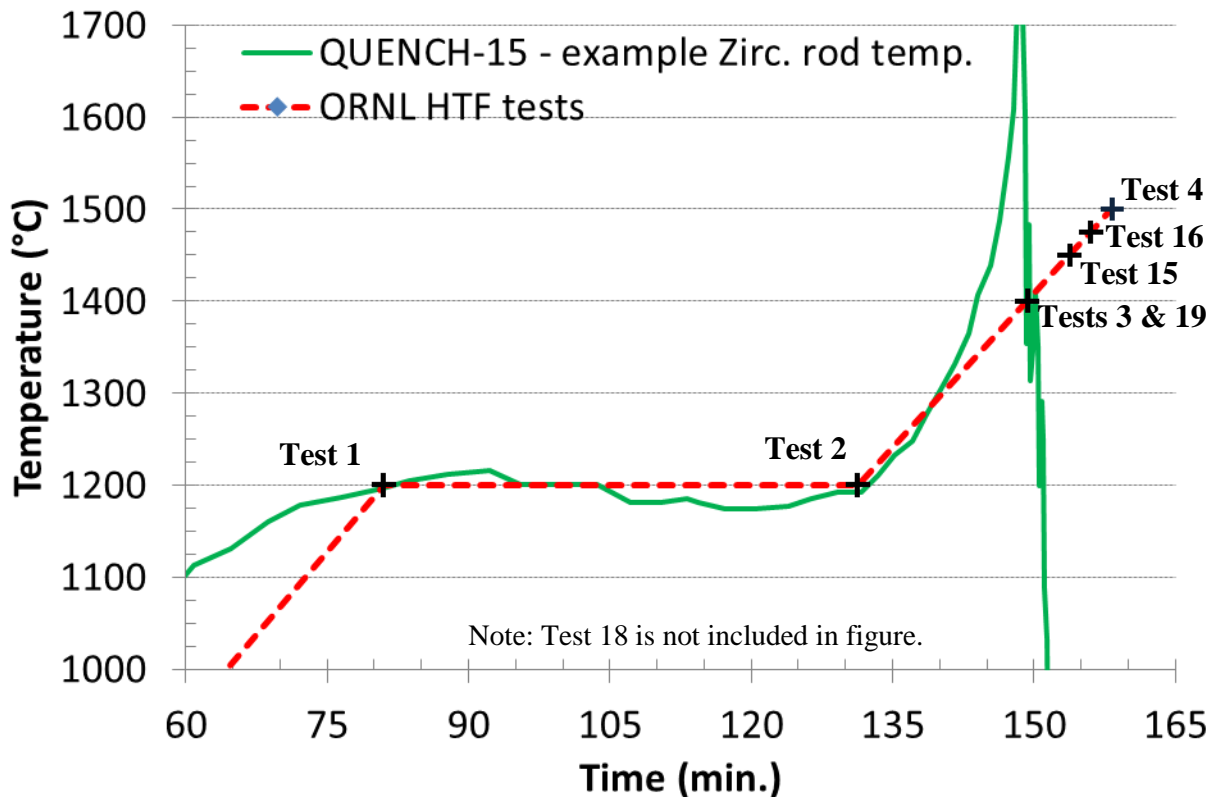
Figure 2. Test endpoints for QUENCH-style oxidation tests.

2.2.2 Test Results

Changes in sample mass pre- and posttest are noted in Table 4 for the eight tests conducted. Posttest images of selected tests are provided in Figure 3. Tests conducted at lower temperatures were visually similar to the nontested cladding.

The high specific mass changes noted for test 16, 59.3 mg/cm^2, and test 4, 62.3 mg/cm^2, indicate substantial attack and degradation of the cladding. If all the aluminum in the sample is assumed to oxidize forming Al_2O_3, the specific mass gain would be approximately 7.0 mg/cm^2. The specific mass gains for

tests 16 and 4 are much higher than this, indicating oxidation of other alloy constituents. Complete oxidation of the sample into Al_2O_3, Fe_3O_4, and Cr_2O_3 (assuming Fe-13Cr-6Al) would result in a weight gain of 55.3 mg/cm^2. The experimental data suggest complete oxidation of the cladding for tests 16 and 4 and the possible formation of other oxides. The cladding degradation for tests 16 and 4 is visually evident in Figure 3. Tests conducted at lower temperatures, 1,450°C and below, have relatively low mass gains (i.e., 1.1% or less of the initial sample mass) and remained intact.

Tests 1, 2, and 18 show the impact of the pre-oxidation phase of the QUENCH test. Only modest oxidation occurs at 1,200°C.

Comparing the repeatability tests 3 and 19, as well as test 15 conducted to a higher temperature, indicates there is some variation between tests. The mass gains and the differences between mass gains are small (i.e., the discrepancies are between small numbers). Possible causes for the discrepancies could be attributed to differences is sample edge conditions (i.e., a small burr or other imperfection), variation in test conditions, and/or minor mass loss during sample handling. Additional repeatability and refinement of oxidation testing is recommended for future work.

Following the temperature ramp conditions of QUENCH-15 and neglecting the rapid exothermic reaction of Zircaloy during the QUENCH-15 test, the HTF tests with B136Y indicate the cladding will remain intact for the anticipated peak temperatures of 1,375-1,400°C in the planned FeCrAl QUENCH test.

Table 4. Test result summary—QUENCH-style tests

Test	Max furnace temp. (°C)	Calc. area (cm^2)	Pre- and posttest mass gain (mg)	Pre- and posttest specific mass change (mg/cm^2)
1	1,200	7.468	1.56	0.209
2	1,200	7.455	1.82	0.244
18[a]	1,200	7.440	2.89	0.388
3	1,400	7.463	6.60	0.884
19	1,400	8.830	12.96	1.468
15	1,450	7.449	4.01	0.538
16	1,475	7.456	442.28	59.32
4	1,500	7.463	464.68	62.26

[a]Test was held at 1,200°C for 150.9 min.
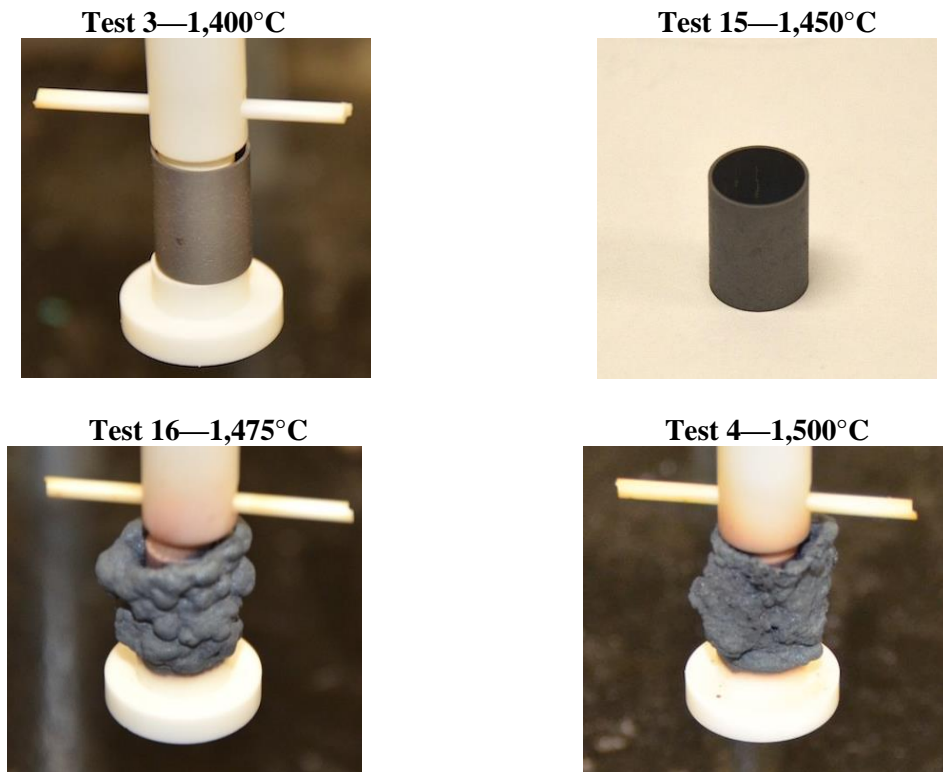
Figure 3. Posttest images of QUENCH-style tests.

2.3 SBO STYLE OXIDATION TEST SERIES

A second set of oxidation tests were conducted based on ramp rates derived from previous MELCOR simulations of boiling water reactor (BWR) station blackout (SBO) scenarios [6]. The objective of the tests was to observe the cladding response during prototypic temperature ramp rates (i.e., more prototypic compared with isothermal tests, past ramps, or the QUENCH-15 ramp sequence). The test data is used in the assessment of the oxidation kinetics for B136Y (see Section 2.4). Also, the tests provide some confirmation of the anticipated cladding performance during simulated and actual severe accident conditions. The tests however did not match the steam flow rate or pressure of the predicted SBO simulations. The cladding was "beginning of life" in that the cladding was neither pre-oxidized in prototypic BWR conditions nor previously irradiated.

2.3.1 Test Procedure

Three simplified temperature histories, based on previous SBO analyses, were applied to the HTF. Each history included three segments. Same as the QUENCH-style tests, the first segment was a ramp at 20°C/min to 600°C in an argon atmosphere with a 1 min hold at 600°C. The second and third segments, where applicable, are provided in Table 5. The tests were stopped after segment 2 or 3.

Table 5. Test segments—SBO-style oxidation tests

Test	Segment 2			Segment 3		
	Ramp rate (°C/min)	Target Temp. (°C)	Hold time at target temp. (min)	Ramp rate (°C/min)	Target temp. (°C)	Hold time at target temp. (min)
7	16.67	1412	1	NA[a]	NA	NA
8	16.67	1412	1	4.17	1500	1
9	7.41	1182	1	NA	NA	NA
10	7.41	1182	1	1.81	1500	1
17	7.41	1182	1	1.81	1550	1
11	5.70	1108	1	NA	NA	NA
12	5.70	1108	1	1.57	1500	1

[a]Not applicable; test stopped after Segment 2.
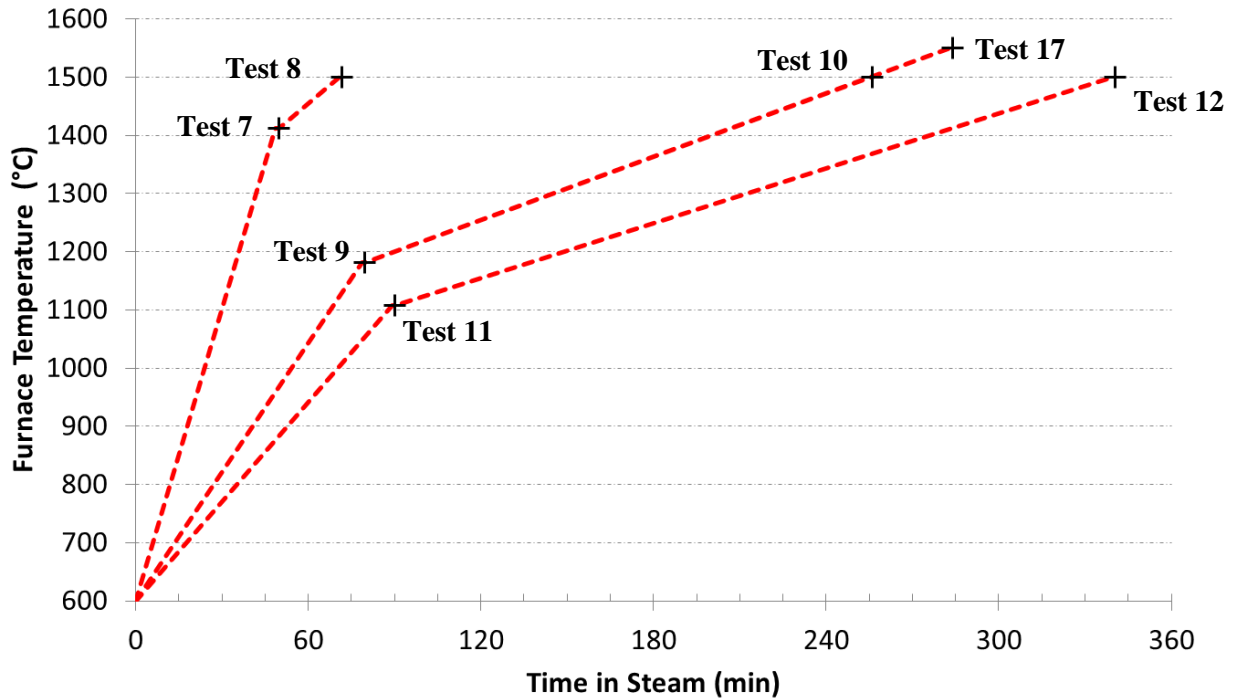
Figure 4. Heating segment illustration for SBO-style oxidation tests.

2.3.2 Test Results

Changes in sample mass pre- and posttest are noted in Table 6 for the seven tests conducted. Posttest images of select tests are provided in Figure 5.

In contrast to the QUENCH-style tests (see Section 2.2), all three tests conducted to 1,500°C did not suffer from substantial attack. Also, interestingly, the posttest appearance of test 17, with a maximum temperature of 1,550°C, is unique from any previous B136Y high-temperature steam oxidation test (see Section 2.2.2 and Ref. [8]). The cladding remained "intact," with no gross signs of melting or change in geometry. However, the pre- and posttest mass measurements indicate a slight loss of mass. Further analysis and testing are required to understand the cladding response at such high temperatures. These

7

results suggest the cladding might stay intact up to 1,500°C under temperature ramp rates predicted for SBO accidents.

Table 6. Test result summary—SBO-style tests

Test	Max furnace temp. (°C)	Calc. area (cm^2)	Pre- and posttest mass gain (mg)	Pre- and posttest specific mass change (mg/cm^2)
7	1412	7.444	3.04	0.408
8	1500	7.441	5.49	0.738
9	1182	7.452	1.07	0.144
10	1500	7.446	7.33	0.984
17	1550	7.448	-0.4	-0.054
11	1108	7.447	1.9	0.255
12	1500	7.435	7.54	1.014

Test 9—1,182°C

Test 10—1,500°C
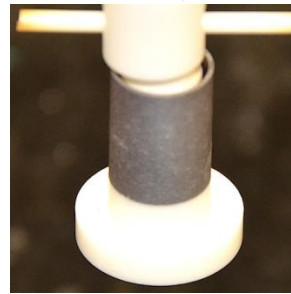
Test 12—1,500°C
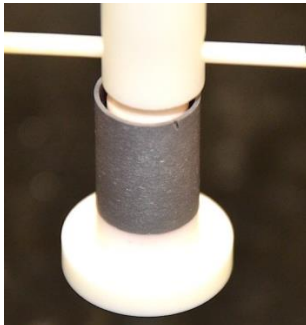
Test 17—1,550°C

Figure 5. Posttest images of SBO-style tests.

2.4 OXIDATION KINETICS EVALUATION

In previous simulation efforts [6], the parabolic oxidation kinetics before the onset of rapid attack were modeled using Eqs. 1 and 2. These kinetics are those previously determined for APMT [3]. After the onset of rapid attack, the default parabolic oxidation kinetics for stainless steel in MELCOR were used [7]. The transition temperature specified for the onset of rapid attack was assumed to be 1,773 K (1,500°C).

$$K(T) = 230 \cdot e^{\left(-41376.0/T\right)} \qquad \text{for T} \leq 1,773 \text{ K ,} \tag{1}$$

and

$$K(T) = (2.42 \cdot 10^9) \cdot e^{\left(-42400.0/T\right)} \qquad \text{for T} > 1,773 \text{ K ,} \tag{2}$$

where

        T = temperature (Kelvin),
        $K(T)$ = reaction rate constant with respect to metal reacted ($kg^2/(m^4 s)$).

Numerically, the mass of reacted metal is evaluated using Eq. 3. To convert metal that has reacted to the oxide produced, it is assumed that aluminum is reacting to form Al_2O_3 for the low-temperature oxidation regime (before Al_2O_3 scale fails) (see Eq. 4). The mass gain can then be determined by the difference between the mass of the oxide formed and the mass of the reacted metal.

$$W_{metal}^{n+1} = \sqrt{\left(\left(W_{metal}^n\right)^2 + K(T^n) \cdot (\Delta t)\right)} ., \tag{3}$$

and

$$W_{oxide} = W_{metal} \cdot \left(\frac{101.964}{2 \cdot 26.982}\right) = W_{metal} \cdot 1.8895 , \tag{4}$$

where

        T   = temperature (Kelvin),
        $K(T)$ = rate constant with respect to metal reacted $kg^2/(m^4 s)$,
        Δt = time step size (s),
        n = the previous time step,
        $n+1$ = the current time step,
        W_{metal} = metal mass reacted (kg),
        W_{oxide} = oxide mass produced (kg).

Based on these relations, the predicted specific mass change for the tests, using the low-temperature oxidation kinetics, is summarized in Table 7 and plotted in Figure 6. Tests 16 and 4 are included and noted in red; however, these two tests experienced substantial attack for which the low-temperature oxidation kinetic is not applicable. Test 17, which was a unique test result with slight mass loss, is also included and noted in red. Two additional test data points are included from previous oxidation testing with B136Y [8]. One data point is from a test in the HTF in which the cladding was ramped from room temperature to 1,400°C in 90 min, with a flowing steam environment of 0.0556 g/s (200 mL/h) for temperatures above 600°C. The other data point is from a test performed in a thermogravimetric analysis device (TGA) that was ramped to 1,480°C at 5°C/min with a steam environment flow at approximately 1 cm/s.

Using Eq. 1, the mass gain is underpredicted for all tests that did not suffer from extensive attack. The leading coefficient in Eq. 1 was increased by factors of 3, 5, and 10. The specific mass changes predicted using the increased oxidation kinetics are provided in Table 7 and plotted in Figure 7 and Figure 8.

By increasing the oxidation rate constant by a factor of 3, the predicted specific mass gain for tests 10 and 12, both SBO-style tests to 1,500°C, align well with the measured data (see Figure 7). However, the rest of the test data is still underpredicted.

When the oxidation rate constant is increased by a factor of 10, the predicted specific mass gain for the tests conducted to higher temperatures (i.e., ≥ 1,450°C) are overpredicted while the lower temperature tests are still slightly underpredicted, Figure 8.

The root mean square deviation (RMSD) of the predicted specific mass changes is 0.500, 0.408, 0.389, and 0.467 for multipliers of Eq. 1 of 1, 3, 5, and 10, respectively (for the 14 tests that did not experience substantial attack). The minimum RMSD was achieved with a multiplier of 5.

Table 7. Measured and predicted oxidation mass change of B136Y

Series	Test	Max furnace temp. (°C)	Specific mass change (mg/cm^2)				
			Measured	Predicted			
				Eq. 1	3 × Eq. 1	5 × Eq. 1	10 × Eq. 1
QUENCH	1	1200	0.209	0.019	0.032	0.042	0.059
	2	1200	0.244	0.061	0.106	0.137	0.194
	18	1200	0.388	0.103	0.179	0.231	0.327
	3	1400	0.884	0.129	0.223	0.288	0.408
	19	1400	1.468	0.129	0.223	0.288	0.408
	15	1450	0.538	0.178	0.309	0.399	0.564
	16	*1475*	*59.32*	*0.211*	*0.366*	*0.472*	*0.668*
	4	*1500*	*62.26*	*0.250*	*0.433*	*0.559*	*0.790*
SBO	7	1412	0.408	0.106	0.184	0.238	0.337
	8	1500	0.738	0.343	0.594	0.767	1.085
	9	1182	0.144	0.019	0.033	0.043	0.061
	10	1500	0.984	0.562	0.973	1.256	1.776
	17	*1550*	*-0.054*	*0.796*	*1.379*	*1.781*	*2.518*
	11	1108	0.255	0.010	0.017	0.021	0.030
	12	1500	1.014	0.602	1.043	1.347	1.905
Ref. [8] HTF	-	1400	0.32	0.090	0.156	0.201	0.284
Ref. [8] TGA	-	1480	0.66	0.290	0.502	0.648	0.917
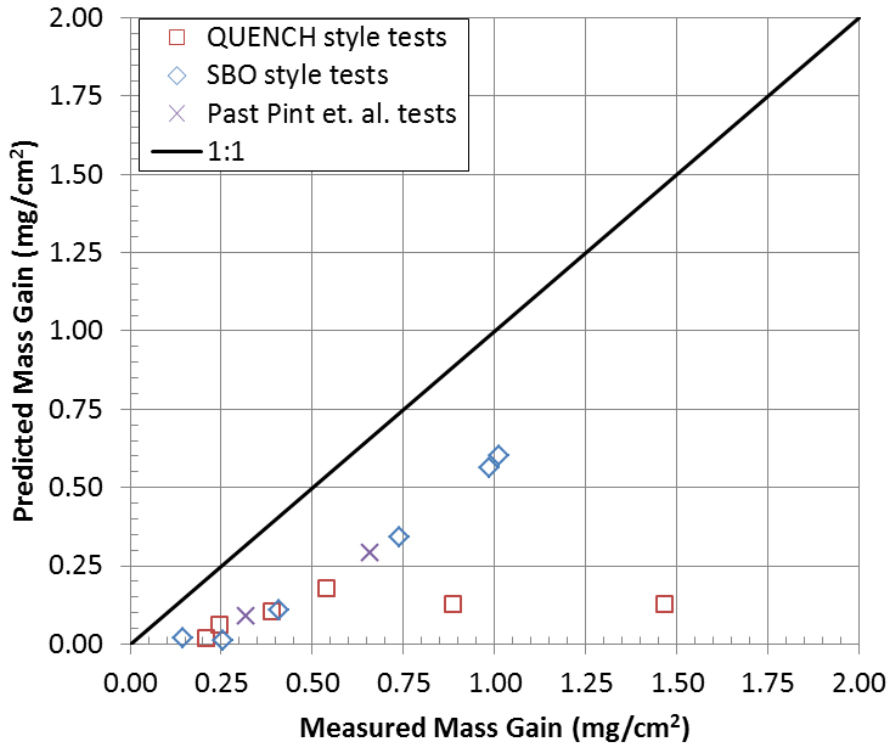
Figure 6. Predicted vs. measured mass gain, using Eq. 1.
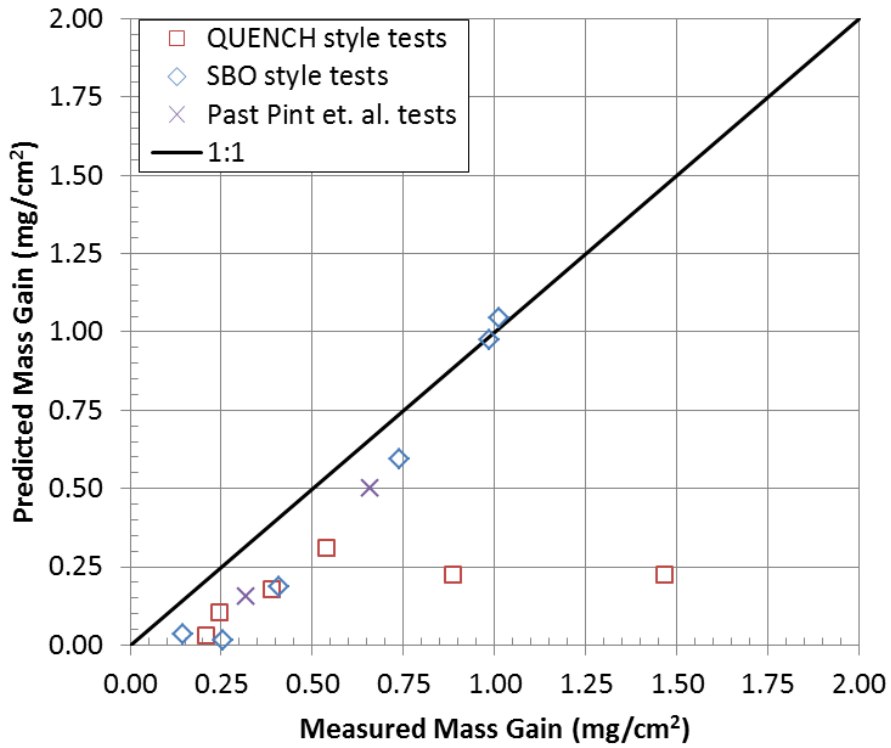
Figure 7. Predicted vs. measured mass gain, using $3 \times$ Eq. 1.
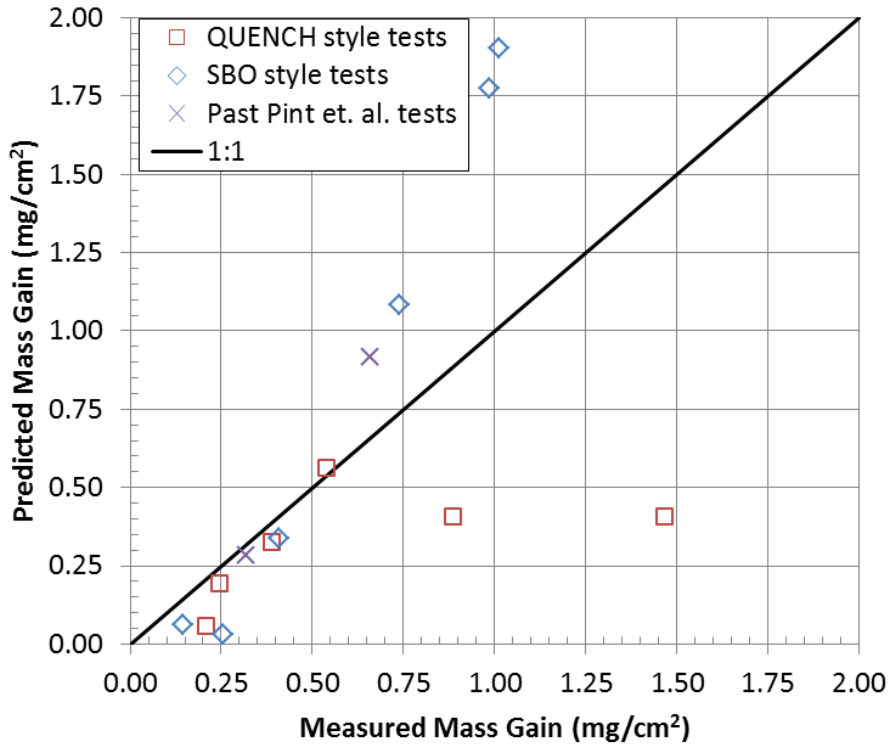
Figure 8. Predicted vs. measured mass gain, using 10× Eq. 1.

2.5 BREAKAWAY OXIDATION ONSET DISCUSSION

At a high enough temperature the cladding suffers from rapid and extensive attack by steam. Evidence of extensive oxidation and melting has been observed in previous tests [8], as well as in the current work (see Sections 2.2.2 and 2.3.2). Figure 9 and Table 8 summarize the B136Y oxidation tests and whether extensive attack was observed. All tests were conducted in the HTF and had 0.0556 g/s (200 mL/h) steam flow rate. In the current study, the B136Y cladding was extensively attacked at 1,475°C and at 1,500°C during the QUENCH-style tests and during a previous test to 1,500°C [8]. However, the cladding reached 1,500°C in all three reactor SBO-style oxidation tests without extensive attack.

Previous simulations [6] used 1,500°C as the transition between low-temperature oxidation kinetics and rapid oxidation at higher temperatures based on the test data for the APMT alloy. The test data for B136Y, a more representative alloy for nuclear reactor applications than APMT, continues to support this transition temperature for SBO-type scenarios.
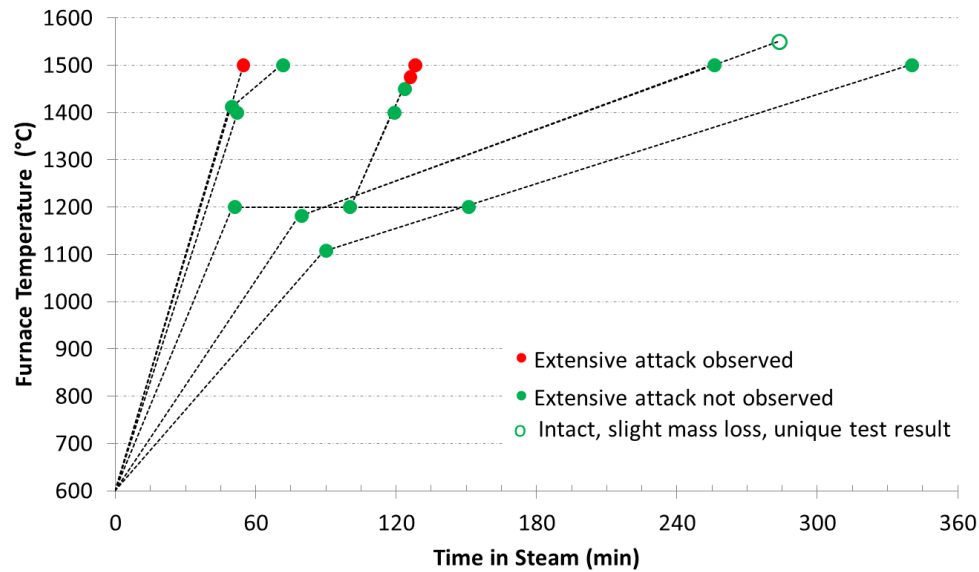
Figure 9. HTF tests with B136Y indicating temperature history and whether extensive attack occurred.

Table 8. Summary of FeCrAl cladding ramp oxidation testing in HTF with 200 mL/h steam flow

Reference	Test number	Alloy	Ramp rate at high temp.(°C/min)	Time above600°C & steam(min)	Melting or accelerated oxidation (°C)						
					1400	1450	1475	1500	1550	1600	1700
Ref [8]	-	B136Y	15.3, 16.4	52.2, 54.7	✓			X			
	7	B136Y	16.67	49.7	✓[a]						
Current work	3, 15, 16, 4, 19	B136Y	11.1	119.3-128.3	✓	✓	X	X			
	8	B136Y	4.17	71.8				✓			
	10, 17	B136Y	1.81	256.1, 283.9				✓	X[b]		
	12	B136Y	1.57	340.6				✓			
				Additional tests							
Ref [8]	-	APM	15.3-19	52-59	✓			✓		X	X
	-	C135M	15.3, 16.4	52.2, 54.7	X			X			

✓ = Melting or accelerated oxidation did not occur.
X = Melting or accelerated oxidation occurred.
[a]Actually went to 1,412°C.
[b]Tube appeared intact but with slight mass loss; unique outcome among tests.

3. ACCIDENT ANALYSIS BACKGROUND AND SETUP

To assess the gains afforded by the FeCrAl ATF concept over the traditional urania fuel–Zr-based cladding system, several SBO severe accident simulations were performed and the results for key figures of merit compared (see Section 4). This section reviews previous analysis efforts, describes the accident scenarios chosen, figures of merit used in the comparison, MELCOR code, plant model, and the modeling of FeCrAl in MELCOR.

Description of the previous work (Section 3.1), figures of merit (Section 3.2), modeling tool (Section 3.3), plant model overview (Section 3.4.1), the modeling of FeCrAl material (Section 3.5), and accident scenario (Section 3.6) are either identical or draw heavily upon work previously documented Ref. [6]. To aid the reader, these sections are included in this report.

3.1 BACKGROUND OF BWR ANALYSES FOR FeCrAl ATF CONCEPT

The first study [9] of the FeCrAl ATF concept during SBO severe accident scenarios in BWRs was based on simulating short-term SBO (STSBO), long-term SBO (LTSBO), and modified SBO scenarios occurring in a BWR-4 reactor with MARK-I containment. The analysis indicated that FeCrAl had the potential to delay the onset of fuel failure by approximately 2.5–6 hours depending on the scenario and to delay lower head failure by approximately 7–7.5 hours. The analysis also indicated reduced in-vessel hydrogen production. However, the work was preliminary and was based on limited knowledge of material properties for FeCrAl. An older version of MELCOR (1.8.5) was used, and limitations of the code were identified for direct use in modeling ATF concepts.

The second study [10] used an updated BWR model for MELCOR 1.8.6 [7] and more representative material properties for FeCrAl. The analysis included unmitigated SBO scenarios (LTSBO and STSBO) as well as mitigated SBO scenarios where water injection was restored to stabilize the accident. For the unmitigated SBO scenarios, the gains were in delaying the accident progression and decreasing the amount of flammable gases generated. The delays ranged from tens of minutes to a few hours (about 4.5 h). Substantially less flammable and noncondensable gasses were generated: 0.6–13.7 tons less by the end of the simulation, depending on the scenario, plus the timing of generation was delayed. The FeCrAl ATF concept provided an additional 1–4.4 hours, depending on the scenario, before radionuclide release to the environment. The results of the mitigated SBO scenarios illustrated the potential benefits of the delayed accident progression and decreased loads on containment. In all three cases analyzed using the FeCrAl ATF concept, the accident was stabilized within 32 hours without deflagrations occurring in the building or releases of radionuclides to the environment. In contrast, for two cases employing Zircaloy, the containment failed, deflagrations occurred in the reactor building, and radionuclides were released into the environment. Containment was predicted not to fail for one Zircaloy case; however, the loads on containment were predicted to be quite high. The simulations demonstrated the advantage of FeCrAl for enhancing the accident tolerance of a plant by affording an opportunity to mitigate and stabilize a severe accident.

A third study [6] incorporated additional insight from materials testing. Previously, the low-temperature oxidation rate equation for FeCrAl (<1,500°C) was implemented over the full range of temperature in the first and second studies. In the third study, this was refined by modeling rapid oxidation of FeCrAl at temperatures above 1,773 K (1,500°C) where the protective oxide layer can fail, as observed during oxidation testing. The analyses use a refined value for the metallic FeCrAl melt point based on experimental work. The analyses also parametrically varied the relocation characteristics of the oxidized FeCrAl based on insight from experimental and theoretical work. A range of mitigated and unmitigated scenarios (7 total) were analyzed. Compared with the second study [10], the gains afforded by the FeCrAl ATF concept over the existing Zircaloy system currently in use were predicted to be less. However, FeCrAl provided gains over Zircaloy in most metrics for all scenarios analyzed with respect to timing and flammable gas generation.

For SBOs, the FeCrAl ATF concept benefits from delayed boil down of the core. The FeCrAl ATF concept delays the onset of cladding collapse by 75–79 min for the STSBO scenario and approximately 3–3.5 h for the LTSBO scenario with dc power loss at 8 hours. For the two scenarios where water injection was maintained for an extended period of time (16 or 24 h) before failure, the FeCrAl ATF concept exhibited much higher gains. For example, employing FeCrAl delayed the onset of cladding collapse by 4–4.7 h and the failure of containment by 4.6–5.2 h. The benefit of the delayed accident progression by the FeCrAl ATF concept was exhibited by the two SBO scenarios where water injection was restored after a specified period of time. In both scenarios the accident was stabilized at an earlier time and at an earlier stage for the FeCrAl cases compared with the Zircaloy cases.

This study expanded upon previous efforts and included a parametric study of the oxidation kinetics for FeCrAl. Select SBO scenarios were simulated with Zircaloy and FeCrAl cladding. Based on the oxidation results with the B136Y alloy (see Section 2.4), the oxidation kinetics developed for APMT were varied by factors of 1, 3, and 10. This study also included modifications to logic within the plant model for operator actions with respect to reactor pressure vessel (RPV) depressurization and high-pressure coolant injection (HPCI) operation. These modifications result in operator actions that are in better alignment with modern guidelines and, therefore, more representative accident scenarios.

3.2 ANALYSIS FIGURES OF MERIT

Key figures of merit, provided in Table 9, were defined related to the timing of the accident progression and flammable gas generation. These are the same used in the previous study [6]; however, the total flammable gas generation is recorded at the end of the simulation, which varies among accident scenarios.

Table 9. Figures of merit descriptions

	Figure of merit	Significance
Timing	0.5 kg of H_2 generated	Onset of hydrogen generation
	First fuel failure (cladding gap release)	First release of radionuclides from fuel
	100 kg of H_2 generated	Significant combustible gas generated
	First cladding metal melting	Degradation of coolable geometry
	First cladding collapse	Degradation of coolable geometry
	Lower head failure	Escalation of accident to ex-vessel
	Containment failure	Loss of radionuclide barrier
	First deflagration in building	Escalation of accident
	0.5 kg of noble gas released to environment	Onset of radionuclide release to outside
Total mass	H_2 gas generated by end of simulation	Flammable gas potential
	CO gas generated by end of simulation	Flammable gas potential

3.3 OVERVIEW OF TOOLS

MELCOR is a system-level code that models the progression of severe accidents in light water nuclear power plants. It was developed and has been maintained by Sandia National Laboratories for the US Nuclear Regulatory Commission. The code encompasses various phenomena that can occur during a severe accident, including thermal-hydraulic response; heat up, degradation and relocation of the core material; transport of radionuclides; and hydrogen generation and combustion. MELCOR is primarily used to estimate the source term from severe accidents.

Previous preliminary simulations [9] of the FeCrAl ATF concept were performed using MELCOR 1.8.5. A number of modeling improvements are included in MELCOR 1.8.6 [7]. One key modeling improvement is the treatment of the reactor vessel bottom head. MELCOR 1.8.6 is still widely used internationally. From version 1.8.6 to 2.1, the major code improvements are primarily related to the code

internal structure; changes were also made to the code input structure. The updates between versions should have limited or no impact on the simulation results of the current study. For the ORNL study, MELCOR 1.8.6(.4073), as compiled by ORNL personnel using the Intel 11.1.064 compiler, was used on a Linux-based computer with Intel-based hardware. MELCOR 1.8.6 was selected because it was made available to incorporate a few minor source code changes required to model FeCrAl. The changes are discussed in Section 3.5.

3.4 PLANT MODEL DESCRIPTION

3.4.1 Overview

The MELCOR plant model used is for Peach Bottom (Unit 2 or 3), a BWR series 4 (BWR/4) with Mark I containment. The model is the same as that used in previous analyses [6] except for the changes noted in Sections 3.4.2 and 3.4.3. The model incorporates all major components, including the reactor, containment, reactor building, various cooling systems (pumps, sprays, piping, tanks), and system and scenario control logic. The model's lineage, and additional model updates have been previously described [11].

The BWR/4 with Mark I containment includes a number of key systems that interact during a station blackout accident. The reactor core isolation cooling (RCIC) system and the HPCI system are steam-driven pumps that can inject water into the RPV. Without other water injection means (from systems relying on ac power or alternate external systems), these systems are used during station blackout as long as dc power remains. The systems have various trip settings, including net positive suction head limits and low steam line pressure. The safety relief valves (SRVs) are located on lines coming off the main steam lines that can vent steam from the RPV to the suppression pool. The suppression pool (aka suppression chamber) is a large water pool located in the torus (aka wetwell) vessel near the bottom of the Mark I containment. Without access to an external ultimate heat sink (resulting from loss of ac power or other events), this pool serves as the heat sink to condense steam being released from the RPV. The rate of containment pressurization is slowed by condensing this steam. However, once the suppression pool becomes saturated (or near saturated) its capability to condense steam is thwarted and the rate of containment pressurization increases.

Within the model, there are different competing failure modes for various structures in the system. Minor differences in accident progression (i.e., resulting from different material properties) can result in different failure modes, causing simulations to vary substantially from one another.

Three competing modes are modeled for lower head failure: thermal failure of a penetration caused by the high temperature of a penetration or the lower head, lower head yielding via creep rupture, and RPV overpressurization. Because overpressurization will not occur during the accident scenarios selected, competition is actually between only failure of a penetration from high temperature and yielding of the lower head.

Four competing failure modes are modeled for the containment. Three are functions of pressure and local temperature and include rupture of the wetwell, rupture of the drywell liner, and leakage of the drywell head flange. The fourth mode is melt-through of the drywell liner from contact with molten core materials. Each failure mode opens different release paths for radionuclides and combustible gases into the reactor building.

3.4.2 Modification of Operator Depressurization Action

In previous simulations, if the suppression pool reached a predefined heat capacity limit, the operators would take action to depressurize the reactor by opening an SRV. However, as modeled, the operators would depressurize the reactor to a point below which the RCIC and HPCI systems would trip from low steam pressure. This resulted in the RCIC and HPCI being isolated around 4.4 h into the accident for

simulation scenarios 2-5 and 7 in Ref. [6]. In reality, however, operators would take action to depressurize the reactor but maintain sufficient steam pressure to allow for continued operation of the RCIC or HPCI.

The logic in the MELCOR model has been modified to prevent operators from depressurizing the RPV below the isolation trip point of the RCIC and HPCI because of low steam pressure. This enables extended operation of the RCIC and HPCI systems.

3.4.3 Modification of HPCI Actuation Logic

In previous simulations, the models for the RCIC and HPCI contained logic that could cause both systems to actuate (i.e., turn on and off) at the same time. This resulted in cyclic periods of large steam draw and rapid refill of the RPV. In reality, operators can take action to use one system or the other at any given time. An additional user option has been added to the model to prevent HPCI operation while the RCIC is available for operation. This option prevents the RCIC and HPCI systems from operating at the same time.

3.5 MODELING FeCrAl ATF CONCEPT IN MELCOR

The FeCrAl material was modeled in MELCOR by replacing the material properties for the zirconium and ZrO_2 materials with those of FeCrAl and FeCrAl oxide. With this approach, the oxide, which is composed of various species, is modeled as a single material with effective bulk properties and degradation behavior.

Workers at Idaho National Laboratory recently developed a separate version of MELCOR 1.8.6 that has a built-in cladding option for the FeCrAl material. However, the this option has not been extended to include the channel box material.

3.5.1 Thermophysical Properties

The density, thermal conductivity, specific heat, and enthalpy for metallic FeCrAl (see Figure 10), were modeled after Kanthal APM [12]. The high-temperature properties were linearly extrapolated to 2,000 K from the available data and held constant for temperatures above 2,000 K. The heat of fusion was assumed to be 275 kJ/kg.

The oxide properties are summarized in Table 10. The density is assumed to be 5180 kg/m^3, which is representative of Fe_3O_4 and is also the default MELCOR value for stainless steel oxide. The thermal conductivity is assumed to be 4.0 W/m K and is representative of Fe_3O_4. The specific heat was modeled as a function of temperature based on weight averaging of the individual Fe_3O_4, Cr_2O_3 and Al_2O_3 oxides assuming a base material composition of 82 wt % Fe-13Cr-5Al. The heat of fusion was estimated to be 664 kJ/kg based on a weight averaging of the individual Fe_3O_4, Cr_2O_3, and Al_2O_3 oxides assuming 82 wt % Fe-13Cr-5Al FeCrAl. The specific heat was modeled as 900.0 J/kg K. With respect to enthalpy, the heat of fusion was applied at melting point temperature. As discussed in Section 3.5.4, the melting temperature for the FeCrAl oxide was parametrically varied.

Table 10. Material properties for FeCrAl and FeCrAl oxide

Assumed material properties	FeCrAl	FeCrAl oxide
Melting point (K)	1,804	Parametrically varied 1870, 1880, 1973
Heat of fusion (J/kg)	275,000	663,867
Density (kg/m^3)	Kanthal APM (Figure 10)	5,180
Thermal conductivity (W/m K)		4.0
Specific heat (J/kg K)		900.0
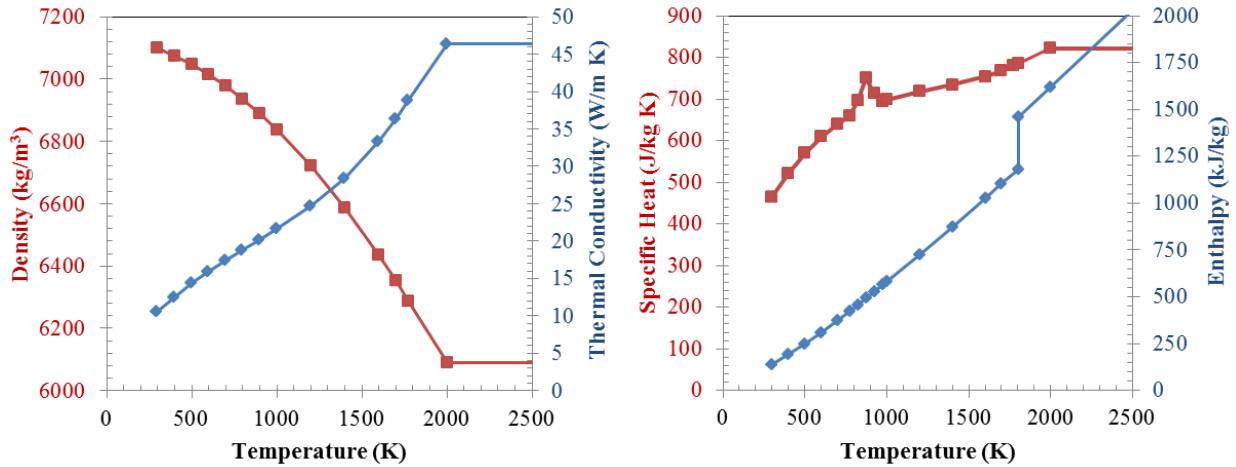
Figure 10. Modeled FeCrAl properties: density and thermal conductivity; specific heat and enthalpy.

3.5.2   Oxidation

As discussed in Section 2.4, the oxidation kinetics of the FeCrAl APMT alloy with steam while in vessel can be modeled by Eqs. (1–4) where K(T) is the oxidation rate constant based on the mass of metal consumed during oxidation. A temperature of 1,773 K (1,500°C) was used previously [6] for the transition between the slower oxidation kinetics, when the Al_2O_3 scale remains protective, and the faster oxidation kinetics when the Al_2O_3 scale fails and there is rapid oxidation of the base metal.

Based on the testing discussed in Section 2, the oxidation kinetics for APMT might underpredict the oxidation of a more prototypic alloy for reactor applications, such as B136Y. To investigate the potential effects of higher oxidation kinetics, simulations were conducted with parametrically varying the low-temperature oxidation kinetics. The tests data, Section 2.5, continues to support a transition temperature of 1,773 K (1,500°C) for the onset of rapid oxidation.

Consistent with previous simulation efforts [6], the oxidation kinetics of FeCrAl with oxygen while in vessel were based on the kinetics of Zircaloy reaction with oxygen but reduced by three orders of magnitude. However, the reaction of FeCrAl with O_2 while in vessel has limited importance during in-vessel core degradation for the accident scenarios chosen. The heat of oxidation for zirconium- and steel-based materials is hardcoded in MELCOR. To more accurately reflect the FeCrAl material, the heat of oxidation for reaction of FeCrAl with H_2O and O_2 was modified in the MELCOR source code. The modification was performed to reflect FeCrAl comprised of 73 wt % Fe-22Cr-5Al with production of Fe_3O_4, Cr_2O_3 and Al_2O_3 oxides. The heat of reaction (at 298 K) for FeCrAl was taken to be 1.247 MJ/kg for reaction with H_2O, and 8.837 MJ/kg for reaction with O_2. Note that a more representative alloy composition for reactor application, 82 wt % Fe-13Cr-5Al, has a lower heat of reactions of 0.9897 MJ/kg with H_2O and 8.451 MJ/kg with O_2. The oxidation reaction equation for MELCOR's zirconium material was modified to reflect the stoichiometry of oxidizing FeCrAl with a composition of 73 wt % Fe-22Cr-5Al. The FeCrAl cladding emissivity, as a function of oxide thickness, was modeled the same as the default in MELCOR for Zircaloy. However, the maximum emissivity of oxidized cladding was set to 0.70.

3.5.3   Core Component Geometry

The cladding thickness was reduced by 50% while maintaining the cladding outer diameter, resulting in 43% less cladding material mass than in the base case. The channel box dimensions remained constant. The gap between the fuel pellet and cladding was assumed to be zero in both the UO_2-FeCrAl and UO_2-Zircaloy models. The fuel pellet outer diameter was increased to offset the reduction in cladding thickness, resulting in the UO_2 mass increasing by 18.5%. The reduction in cladding thickness is based on previous reactor physics assessments of FeCrAl cladding in pressurized water reactors in which it was determined that maintaining operational cycle lengths was best accomplished through a small increase in batch-average enrichment and reduction of the cladding thickness to about half of the nominal thickness [13, 14, 15]. Recent neutronics studies found similar results for BWRsand suggest reducing both the cladding and channel box thicknesses by about 50% [16, 17]. Reducing the channel box thickness impacts core thermal hydraulics with respect to flow area. Modeling a reduced channel box thickness is left for future work.

Modeling of the control blades was unmodified. They are composed of B_4C and stainless steel. The simple oxidation model for B_4C was employed in MELCOR.

3.5.4   Fuel Degradation and Relocation Characteristics

For Zircaloy cladding, there are numerous tests on its behavior under accident conditions [18], including the heating up, burst, oxidation, melting, and relocation of the cladding. MELCOR simulates the burst of the rods and models oxidation of the cladding, buildup of oxide thickness, melting/candling of the metallic Zircaloy, collapse and rubblization of the oxidized cladding, etc., as well as modeling the heating up and melting of the other core structures (channel box, control blades, etc.). MELCOR contains a number of melting temperatures and relocation conditions that can be modified by the user.

Failure and relocation of a FeCrAl clad fuel rod under accident conditions still remains to be experimentally investigated. The following four sections describe modeling for the various failure modes for Zircaloy and FeCrAl. The temperatures used for these failure modes are summarized in Table 11.

Table 11. Summary of failure temperatures

Cladding case	Rod burst onset (K)	Melting		Oxide forced failure	
		Metal (K)	Oxide (K)	Shell melt holdup (K)	Collapse (K)
Zircaloy	1,173	2,098	2,990	2,400	2,800
FeCrAl	1,173	1,804	1,880	1,870	1,870

3.5.4.1   Burst

For both Zircaloy and FeCrAl cladding, the rods are assumed to burst and release their radionuclides residing in the gap at 900°C. In reality, the rod burst phenomenon is a function of both rod pressure and temperature. The burst characteristics of first-generation FeCrAl alloy claddings have been investigated [19]. For the same hoop stress, the FeCrAl cladding was shown to have improved burst characteristics, (~10% higher burst onset temperature) and different ballooning characteristics (i.e., lower strain).

3.5.4.2   Melting

Based on default MELCOR values, Zircaloy melts at 2,098 K (1,825°C) and zirconium oxide at 2,990 K (2717°C) [7]. The melting point for uranium dioxide is set to 2,800 K to capture its lower melting point depending on interactions with other materials.

The melting point of the metallic FeCrAl is modeled as 1,804 K (1,531°C) based on computed values that were experimentally verified at ORNL [6, 20].

The melting point, or effective melting point of the oxide structure, was also previously investigated [6, 20] with no clear evidence of oxide melting up to the 1,973 K (1,700°C) conditions tested (Ar-20% O_2 atmosphere). The melting points of the individual oxides, Al_2O_3 or Cr_2O_3, are quite high, more than 2,273 K (2,000°C). However, the melting points of Fe_3O_4 (~1,597°C) [7] and FeO (~1,377°C) and the decomposition temperature of Fe_2O_3 (~1,539–1,565°C) are quite low compared with zirconium oxide. However, test data for the effective melting point of the FeCrAl oxide under prototypic steam conditions is not available. Previously, the melting temperature of the FeCrAl oxide was parametrically varied between 1,870 and 1,973°C for a range of BWR SBO accident scenarios [6]. For the current work, the melting point of the oxide was assumed to be 1,880 K (1,607°C), 10 degrees higher than the melting point of Fe_3O_4.

3.5.4.3 Eutectics

The formation of eutectics greatly influences the core degradation process in existing reactors using Zircaloy [7]. Note that B_4C and steel, relevant for the control blades, have a eutectic modeled as 1,420 K (1,147°C) in MELCOR. Bechta et al. found a eutectic between FeO and UO_2 at 1,610 K (1,337°C) [21]. In discussion of the PHEBUS tests [22], the potential for FeO_x to interact with UO_2 was noted. Previous separate effects tests that used a UO_2 crucible loaded with FeO powder experienced rapid penetration of the FeO into the UO_2 under the 1,673 K (1,400°C) inert atmosphere test conditions [23]. The potential eutectic formation of FeCrAl with B_4C, stainless steel, Inconel, and UO_2 needs to be investigated in the future. MELCOR includes an option to model the formation of eutectics and the dissolution of one material by another. However, its use is not recommended by default and is not included in this modeling effort for the Zircaloy or FeCrAl simulations.

3.5.4.4 Other collapse and failure modes

MELCOR includes a failure mode that allows the cladding to remain standing up to a specified temperature if the cladding is fully oxidized. The code also includes a failure mode that forces collapse of the rods based on a time-at-temperature criterion. Finally, the code models the ability for an oxide shell to hold up melt.

For Zircaloy, once the cladding exceeds 2,400 K, the time-at-temperature criterion for cladding failure is activated. The cladding is modeled to remain intact only for a specified amount of time depending on the temperature. This is included in the model to preclude very hot, or once very hot, cladding from standing indefinitely. A fully oxidized cladding is modeled to remain standing (pending the time-at-temperature failure mode) until 2,800 K. More recent code guidelines recommend a value of 2,500 K. However, in all simulations using Zircaloy in Section 4, the cladding collapses at temperatures below 2,500 K. An oxide shell will support a metallic melt at up to 2400 K, above which the shell will fail.

Data for a time-at-temperature failure mode is not available for FeCrAl cladding. Above some temperature, modeled as 1,773 K (1,500°C) for the oxidation kinetics (Section 2.5), the protective Al_2O_3 scale fails and there is continued and rapid oxidation of the iron. Unlike ZrO_2, which can remain structurally intact for some time, iron oxide is unlikely to remain in a rod-like geometry. Indeed, images of heavily oxidized FeCrAl samples (Section 2.2.2 and Ref. [8]) support this postulation. For the simulations, fully oxidized cladding is assumed to fail at 1,870 K, the melting temperature for Fe_3O_4. Because of the lack of experimental data, the time-at-temperature criterion used for Zircaloy was kept for FeCrAl. However, it will not be activated during simulations because the cladding relocates before reaching the high temperature (2,400 K) required.

MELCOR also includes the ability for an oxide shell to hold up melt. A zirconium oxide shell is modeled to remain intact and able to support a melt at up to 2,400 K. As noted, the FeCrAl oxide is unlikely to be structurally sound and is modeled to fail at 1,870 K, the melting temperature of Fe_3O_4.

3.5.5   Radionuclide Inventory and Decay Heat

The core radionuclide inventory and distribution and the total decay heat and distribution were not modified and were the same as the model with zirconium-clad fuel. To date, a reference assembly design has not been developed that can accommodate the integral considerations of thermal hydraulics, neutronics, fuel performance, and economics. Once a FeCrAl ATF fuel assembly design and core loading are developed, the radionuclide and decay heat distributions should be revised.

3.5.6   Note on Ex-Vessel Modeling

The core-concrete interaction modeling in MELCOR is performed by a separate package (based on CORCON-Mod3) with its own material properties. During transfer of melt from in-vessel to ex-vessel, the model was modified to map the zirconium and zirconium oxide materials (modified to model FeCrAl) to stainless steel and stainless steel oxide materials. Thus, the FeCrAl material is treated as stainless steel by the core-concrete interaction modeling. Some insight into the consequences of this can be found in Ref. [24]. Substituting stainless steel (or zirconium) for FeCrAl in the ex-vessel modeling could impact the oxidation rate of the material; however, the oxidation rate is generally limited by the availability of concrete decomposition gases. The substitution impacts the amount of energy generated during oxidation, as well as the amount of hydrogen generated. The substitution will also impact the material properties predicted for the debris. This limitation could be explored and addressed in the future, but it is likely overshadowed by the limited ex-vessel debris coolability models that are integrated into the released MELCOR 1.8.6 and early 2.1 versions [25, 26].

3.6   ACCIDENT SCENARIO AND CASES

3.6.1   Station Blackout Accident Scenarios Modeled

SBO severe accident scenarios were chosen for investigation because of their high contribution to the overall core damage frequency for BWRs [27]. In addition, the accidents that occurred at Fukushima Daiichi Units 1–3 were variants of the SBO scenarios [28].

During the SBO scenarios, the reactor is assumed to successfully trip (reference time 0 h). All ac power, off-site and on-site (diesel generators), is assumed to be lost at 0 h. The timing of the loss of dc power (batteries) was modeled to occur at 0 h (STSBO) and 8 h (LTSBO).

While dc power is maintained, the RCIC and HPCI systems can be used to inject cooling water into the primary system. As modeled, operators do not control the speed of the RCIC or HPCI systems. Thus, the systems turn fully on and off as necessitated by the water level. Also, as modeled, these systems are aligned to take suction from the condensate storage tank.

While RCIC and HPCI operate, the SRVs actuate automatically at their pressure set point. Manual operation of the SRVs relies on dc power and plant air availability. As modeled, the operators will manually depressurize the RPV down to ~1.14 MPa (150 psig), using an SRV, if the suppression pool exceeds its heat capacity limit. Once dc power is lost, the ability to manually actuate the SRVs is lost, and the RPV can repressurize up to the pressure set point for automatic SRV actuation.

After water injection ceases, the RPV water inventory boils away, uncovering the core. The fuel rods heat up, oxidize—generating heat and hydrogen—and begin fail. The failed fuel relocates downward and could eventually fail the lower head of the RPV. This core debris could interact with the concrete containment floor, oxidizing metallic species in the debris. Throughout these events, the generation of steam and noncondensable gases cause the containment to pressurize. As modeled during the scenarios,

the operators do not take action to vent containment. Eventually, the containment fails, releasing radionuclides and hydrogen into the reactor building. Deflagrations can occur in the reactor building, and radionuclides can ultimately be released into the environment.

Three different external water injection recovery scenarios were considered. In one scenario, water injection into the primary system is not restored (unmitigated STSBO and LTSBO). In the second scenario, water injection occurs through a feedwater line at a rate of 0.417 m^3/min (110 gpm) from 12 to 36 h after the loss of ac power (partially mitigated SBO, or PMSBO). After 36 h, dc power is lost and all water injection ceases. For the third scenario, water injection is restored indefinitely into a feedwater line at a rate of 0.568 m^3/min (150 gpm) beginning 2 h after the loss of dc power (mitigated STSBO, MSTSBO).

3.6.2 Oxidation Kinetics Parametric Study Cases

As discussed in Section 2, FeCrAl alloys being investigated for reactor applications might have higher oxidation kinetics than that of the APMT alloy. In the analysis of the oxidation tests with B136Y (see Section 2.4), the low-temperature oxidation kinetics (i.e., before the transition to rapid oxidation) of APMT were found to underpredict the total oxidation. Increasing the APMT oxidation rate constant by a factor of 3 enabled reproduction of two of the SBO-style tests conducted to 1,500°C. Increasing the APMT oxidation rate constant by a factor of 10 more closely predicted the oxidation of the lower temperature/less oxidized samples but overpredicted a number of the tests. Finally, increasing the APMT oxidation rate constant by a factor of 5 resulted in the best agreement with the data set with respect to the overall RMSD value.

To investigate the impact of the FeCrAl oxidation rate on the accident progression, the oxidation rate was parametrically varied. The low-temperature oxidation kinetics rate constant of APMT was increased by factors of 1, 3, and 10 (see Table 12 and Eq. 1). Included in the table are the values for the Zircaloy low-temperature oxidation rate used in the MELCOR model and the transition temperature to the high-temperature oxidation rate.

Table 12. Case variations of low-temperature steam oxidation kinetics

Cladding case	Constant coefficient $(kg^2_{metal}/(m^4 \cdot s))$	Exponential term (K)	Transition temp. (K)
Zircaloy	29.6	16,820.0	1,853
FeCrAl-1× Oxid.	230.03	41,376.0	1,773
FeCrAl-3× Oxid.	690.09	41,376.0	1,773
FeCrAl-10× Oxid.	2300.3	41,376.0	1,773

3.6.3 Simulation Summary

The simulations analyzed in Section 4 are summarized in Table 13. Four SBO scenarios are considered, and for each scenario a Zircaloy base case is simulated as well as three FeCrAl cases with varying low-temperature oxidation kinetics.

Table 13. Summary of scenarios and cases

Scenario type	Accident scenario	Report section	Timing of dc power loss (h)	External water injection		Simulation end time (h)	Oxidation kinetics case (see Table 12)
				Timing (h)	Rate (L/min)		
Unmitigated STSBO	1	4.1	0	Never	NA[a]	16	Zircaloy FeCrAl 1× Oxid. FeCrAl 3× Oxid. FeCrAl 10× Oxid.
Unmitigated LTSBO	2	4.2	8	Never	NA	32	Zircaloy FeCrAl 1× Oxid. FeCrAl 3× Oxid. FeCrAl 10× Oxid.
Delayed SBO with mitigation failure (PMSBO)	3	4.3	36	12–36	417	72	Zircaloy FeCrAl 1× Oxid. FeCrAl 3× Oxid. FeCrAl 10× Oxid.
MSTSBO	4	4.4	0	2–end of sim.	568	32	Zircaloy FeCrAl 1× Oxid. FeCrAl 3× Oxid. FeCrAl 10× Oxid.

[a]NA = not applicable.

4.   ANALYSIS RESULTS

Sections 4.1-4.4 present the simulation results for each scenario. Key results are summarized in Section 4.5.

4.1   UNMITIGATED STSBO

The figures of merit results for these cases are summarized in Table 14. Figure 11 through Figure 16 depict the reactor and containment pressure, RPV water level, peak intact cladding temperature, fraction of cladding collapsed, and the total and in-vessel hydrogen generation.

During the unmitigated STSBO, there are no operator actions or water injection by the RCIC, HPCI, or external means. Without operator actuation of the SRVs or the RCIC/HPCI operating, the RPV remains pressurized until the RPV lower head fails. The RPV water level continuously drops as the water boils away. The lower head dries out faster and fails sooner in the FeCrAl cases than the Zircaloy case. This is likely attributed to the timing of debris relocation to the lower head, the degree of material superheat and oxidation during relocation, and the lower melting point of the metallic and oxidic FeCrAl material. The failure of the RPV and subsequent core debris-concrete interaction results in failure of the containments. Soon after containment failure, deflagrations are predicted to occur in the secondary containment and noble gases (and other radioactive fission products) are released to the environment. The outer ring of FeCrAl assemblies is predicted to remain standing for an extended period; however, during previous simulations [6], the outer ring eventually fails and relocates downwards.

In general, the accident progressed at similar rates for the three FeCrAl cases (see Table 14). The difference in the low-temperature oxidation kinetics for FeCrAl did result in minor differences in hydrogen generation (see Figure 16). However, this difference was insignificant with respect to significantly influencing the subsequent accident progression. This is examined in further detail for the LTSBO in Section 4.2.

When comparing the figures of merit of the three FeCrAl cases to the base case Zircaloy system, the onset of hydrogen generation is delayed from 37 to 39 min. The timing to first release of the radionuclides in the gap is delayed only 4 min. The generation of substantial quantities of hydrogen (taken as 100 kg) is delayed by 84 min. The timing to initial melting of the metallic cladding is delayed 75 min, and the initial collapse of a cladding segment is delayed 79 min. After the onset of fuel damage, the FeCrAl cases exhibit a more rapid lower head failure, containment failure, and occurrence of deflagrations in the reactor building. All the FeCrAl cases produce slightly less hydrogen and less carbon monoxide by 16 h.

Table 14. Figure of merit results for unmitigated STSBO

Figure of merit	Zircaloy	FeCrAl 1× Oxid.	FeCrAl 3× Oxid.	FeCrAl 10× Oxid.
0.5 kg of H_2 generated[a]	70	109	108	107
First fuel failure (gap release)[a]	72	76	76	76
100 kg of H_2 generated[a]	97	181	181	181
First cladding metal melting[a]	112	187	187	187
First cladding collapse[a]	112	191	191	191
Lower head failure[a]	568	506	515	519
Containment failure[a]	582	532	553	539
First deflagration in building[a]	582	532	553	539
0.5 kg noble gas release to environment[a]	571	532	554	539
H_2 gas generated by 16 h[b]	2,500	2,201	2,269	2,057
CO gas generated by 16 h[b]	16,175	11,375	10,162	11,465

[a]Measured in minutes.
[b]Measured in kilograms.
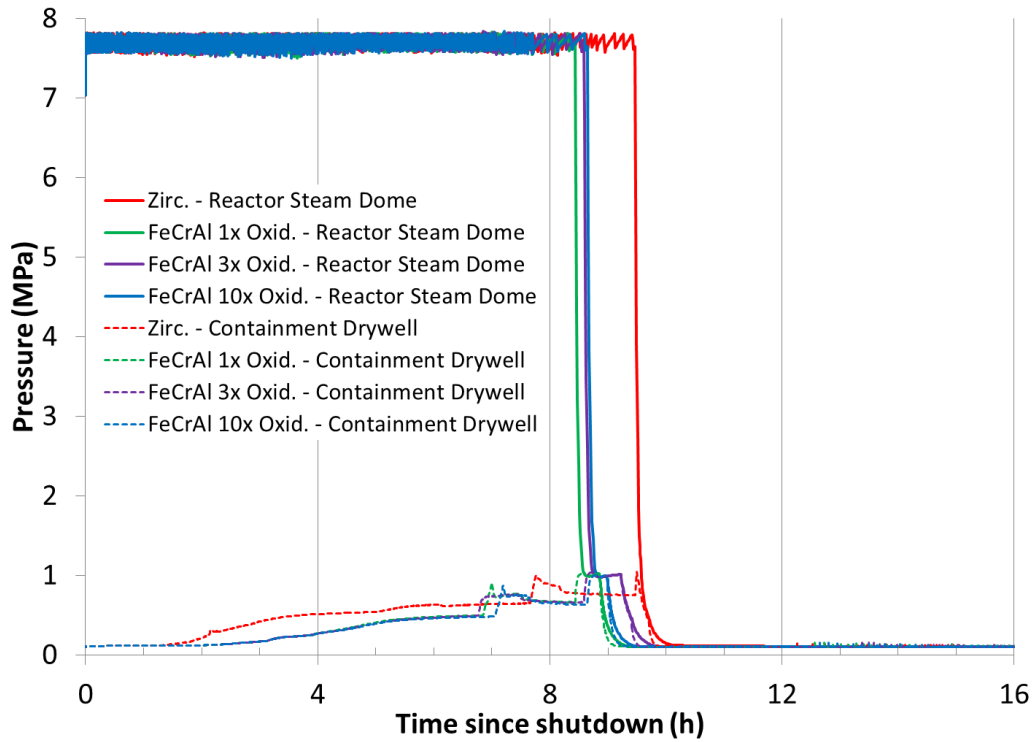
**Figure 11. STSBO–Reactor and containment pressure.**
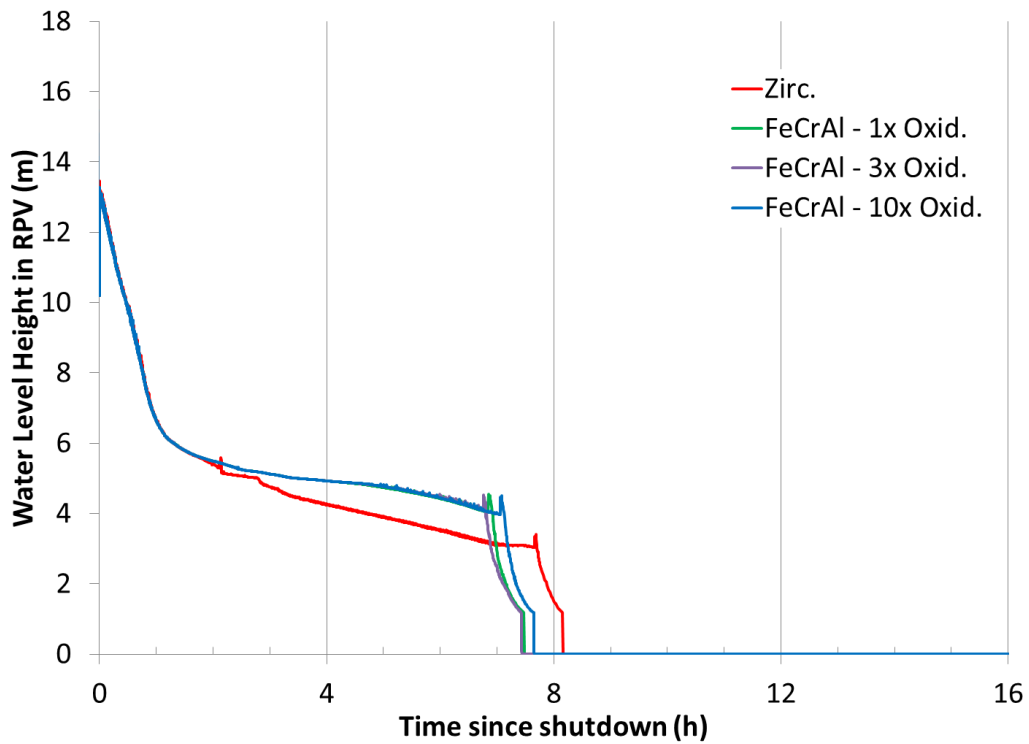

Figure 12. STSBO–RPV water level.
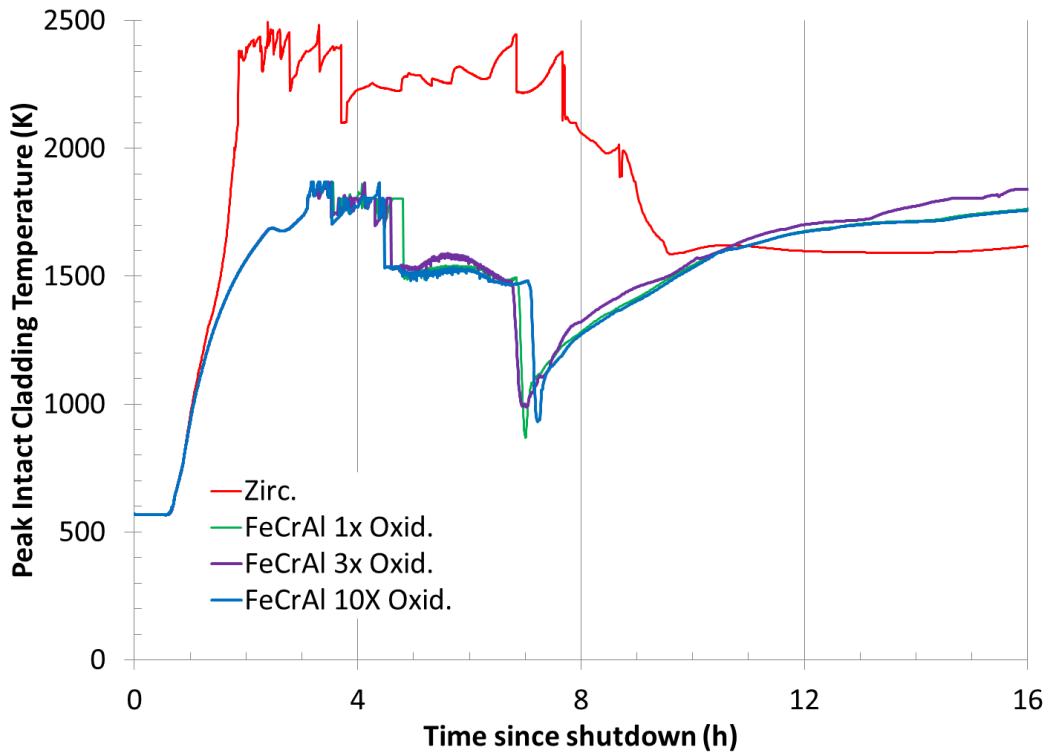
**Figure 13. STSBO–Peak intact cladding temperature.**
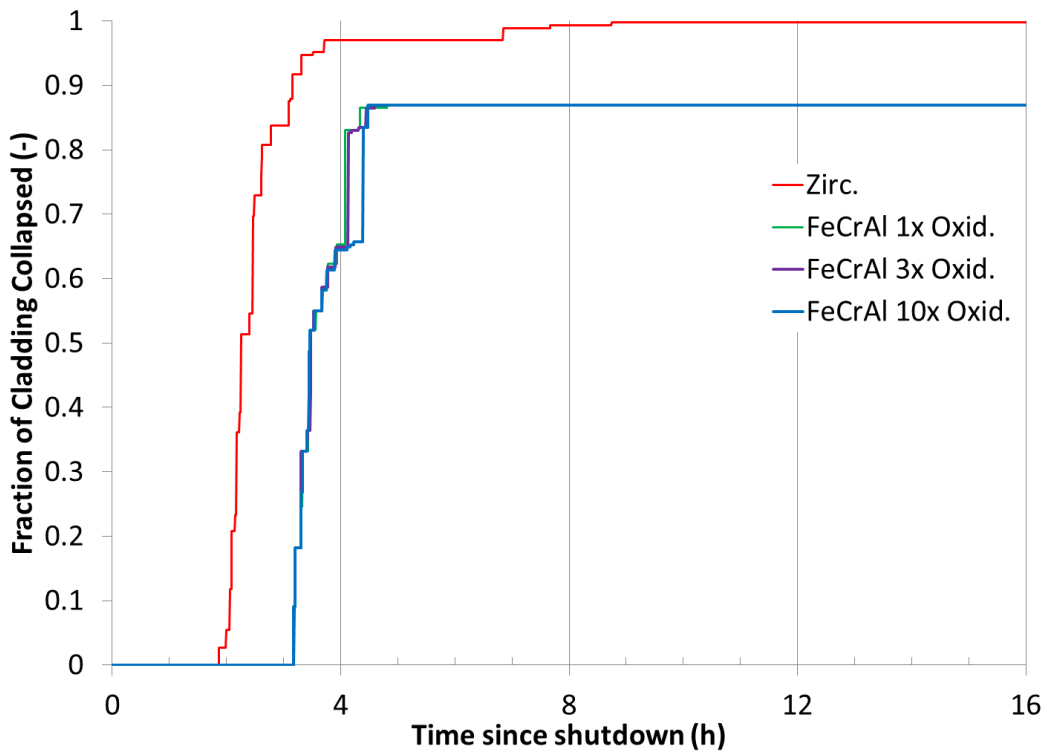
**Figure 14. STSBO–Fraction of cladding relocated.**
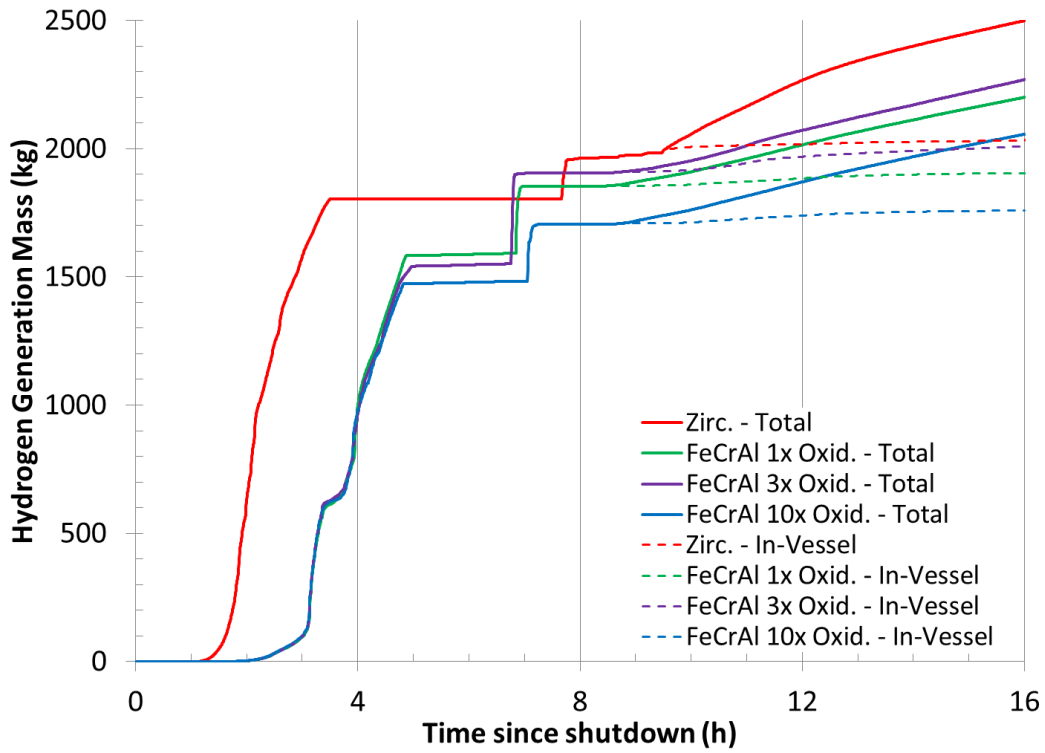
**Figure 15. STSBO–Hydrogen generated in-vessel and total.**
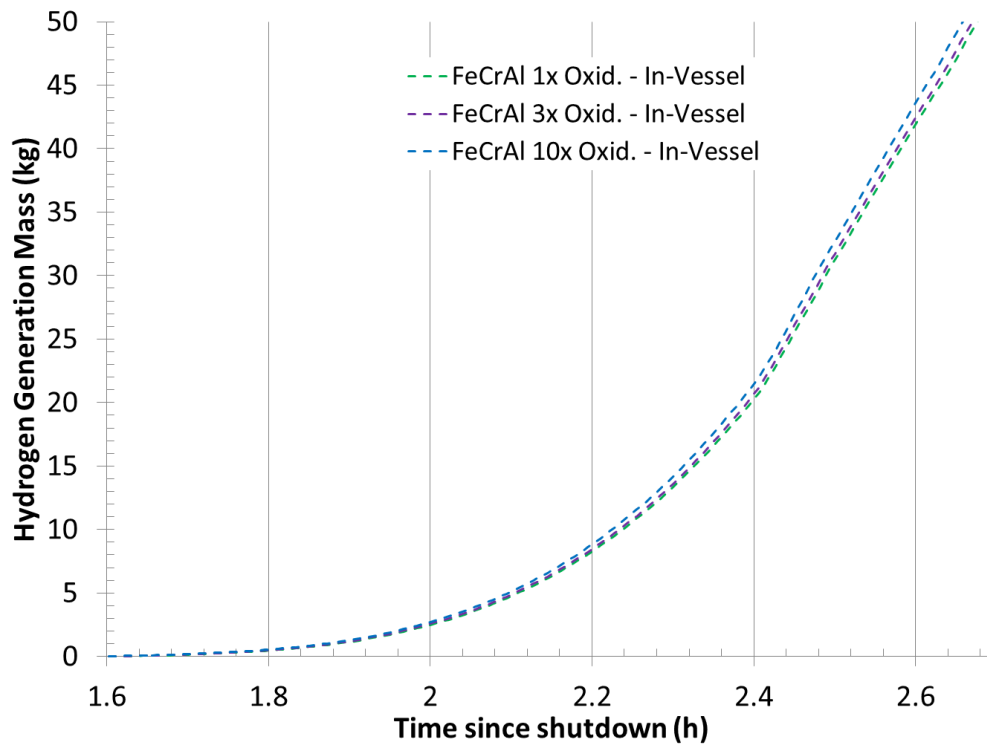
Figure 16. STSBO–FeCrAl in-vessel oxidation comparison.

4.2   UNMITIGATED LTSBO WITH DC LOSS AT 8H

The figures of merit results for the cases are summarized in Table 15. Figure 17 through Figure 24 depict the reactor and containment pressure, RPV water level, peak intact cladding temperature, fraction of cladding collapsed, and the total and in-vessel hydrogen generation.

During the unmitigated LTSBO, the operators have dc power for 8 h. As modeled, the operators depressurize the RPV at 2.9 h by manually actuating an SRV because of high temperatures in the suppression chamber. The RCIC operates cyclically to maintain RPV water level until 8 h when dc power is lost. Once dc power is lost, the manually controlled SRV closes and the RPV repressurizes up to the lowest automatic set point of the SRVs. As the RPV repressurizes, the water level briefly swells and then resumes boiling away. Eventually, the fuel become uncovered and begins to heat up. The Zircaloy cladding heats up faster than the FeCrAl cladding because of the oxidation kinetics. Despite its higher failure temperature, the Zircaloy cladding begins to relocate much sooner than the FeCrAl cladding. The containment is predicted to fail earlier in the Zircaloy case than in the FeCrAl cases. The earlier hydrogen generation and heat generated during oxidation of the Zircaloy contributes to the earlier pressurization and failure of containment. Soon after containment failure, deflagrations are predicted to occur in the secondary containment and noble gases (and other radioactive fission products) are released to the environment. The core debris relocates downward, eventually into the RPV lower head. The lower head dries out and fails faster in the Zircaloy case than in the FeCrAl cases. The melt relocates to the drywell where core debris-concrete interaction is predicted to occur.

In general, the accident progressed at similar rates for the three FeCrAl cases (see Table 15). The difference between the FeCrAl cases grows as the accident progresses. As shown in Figure 22, the oxidation rate of the FeCrAl (cladding and channel box) is initially quite low compared with the Zircaloy case. In fact, the oxidation of the control blade (B4C and stainless steel) is initially the primary source of hydrogen generation in the FeCrAl case while oxidation of Zircaloy (cladding and channel box) dominates for the Zircaloy case. For the FeCrAl cases, it is only after FeCrAl reaches the transition to the high-temperature oxidation kinetics that the oxidation of the FeCrAl becomes the dominate source of hydrogen generation (see Figure 23). The scaling of FeCrAl's low-temperature oxidation rate constant affects the FeCrAl oxidation (i.e., it is verified that the code is capturing the effect), as shown in Figure 24. However, the oxidation of FeCrAl (even with factors of 3 and 10 higher rate constants) is negligible compared with the oxidation of the control blades early in the scenario. Even with a 100 times higher low-temperature oxidation rate constant, the oxidation of the FeCrAl is a small contributor to the total generation before the transition to the high-temperature oxidation kinetics.

The figures of merit (Table 15) show that when comparing the three FeCrAl cases with the base case Zircaloy system, the onset of hydrogen generation is delayed 71–73 min for the FeCrAl cases. The timing to first release of the radionuclides in the gap is delayed only 7 min. The generation of substantial quantities of hydrogen (taken as 100 kg) is delayed by 200–202 min. The timing to initial melting of the metallic cladding is delayed ~195 min, and the initial collapse of a cladding segment is delayed 200–211 min. Following fuel failure, the difference between FeCrAl cases increases. Lower head failure is delayed 68–168 min, containment failure and the start of deflagrations is delayed 133–208 min, and the start of radionuclide release to the environment is delayed 131–208 min. All the FeCrAl cases produce slightly less hydrogen and approximately one-half to one-third of the carbon monoxide by the end of the simulation at 32 h.

Table 15. Figure of merit results for unmitigated LTSBO–8 h

Figure of merit	Zircaloy	FeCrAl 1× Oxid.	FeCrAl 3× Oxid.	FeCrAl 10× Oxid.
0.5 kg of H_2 generated[a]	885	958	958	956
First fuel failure (gap release)[a]	891	898	898	898
100 kg of H_2 generated[a]	939	1,141	1,141	1,139
First cladding metal melting[a]	974	1,169	1,169	1,168
First cladding collapse[a]	975	1,175	1,175	1,186
Lower head failure[a]	1,577	1,645	1,681	1,745
Containment failure[a]	1,399	1,532	1,579	1,607
First deflagration in building[a]	1,399	1,532	1,579	1,607
0.5 kg noble gas release to environment[a]	1,401	1,532	1,580	1,609
H_2 gas generated by 32 h[b]	2,377	2,218	2,249	2,300
CO gas generated by 32 h[b]	8,974	4,618	4,379	2,963

[a]Measured in minutes.
[b]Measured in kilograms.
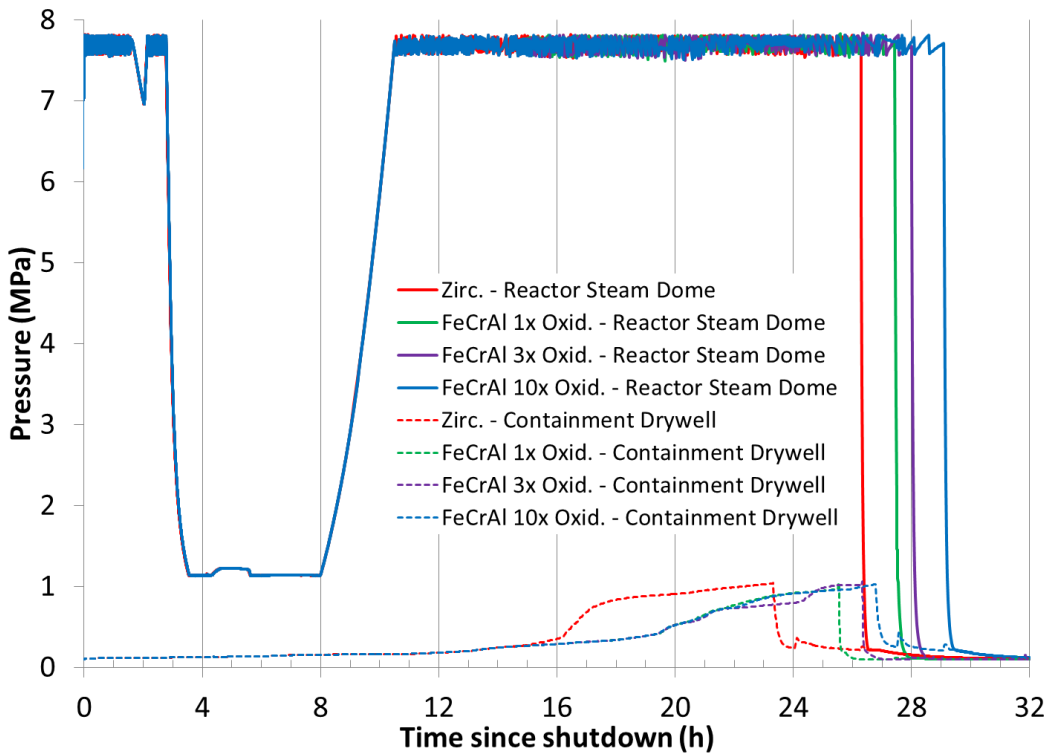
Figure 17. LTSBO–reactor and containment pressure.
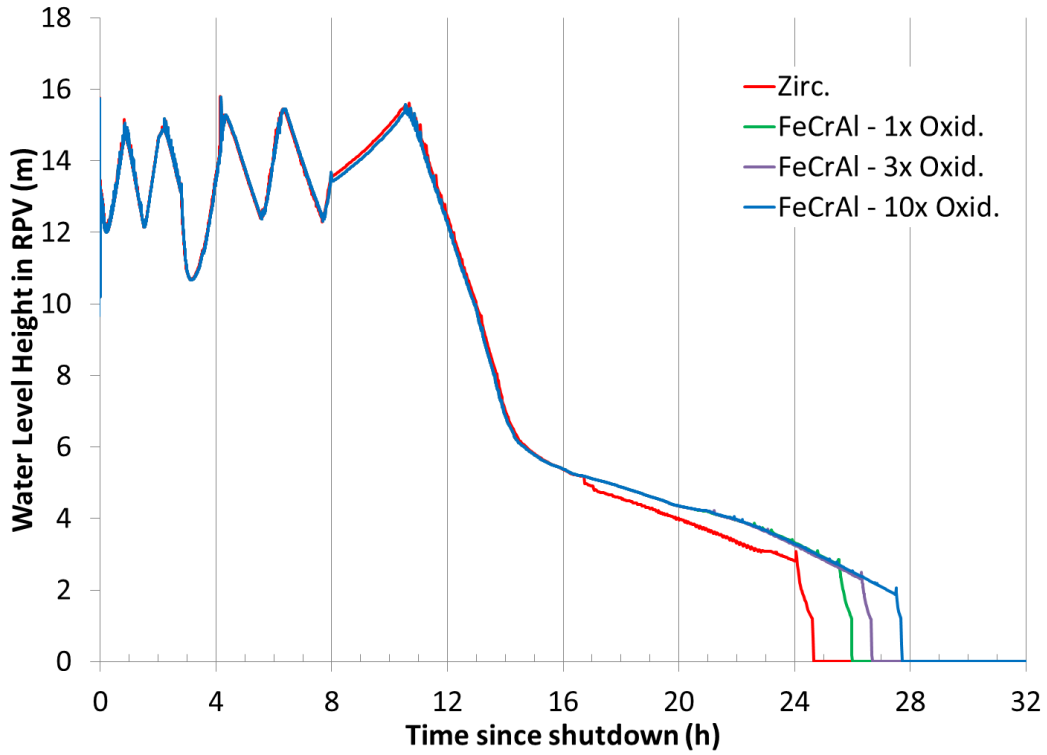
**Figure 18. LTSBO–RPV water level.**
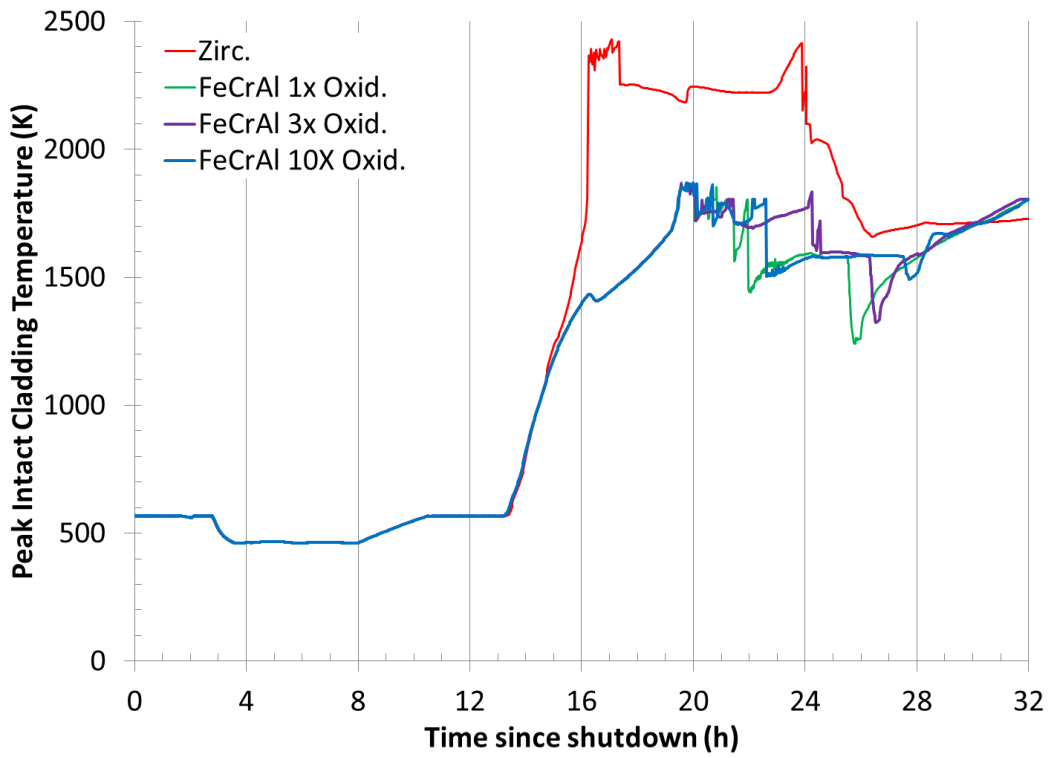
Figure 19. LTSBO–Peak intact cladding temperature.
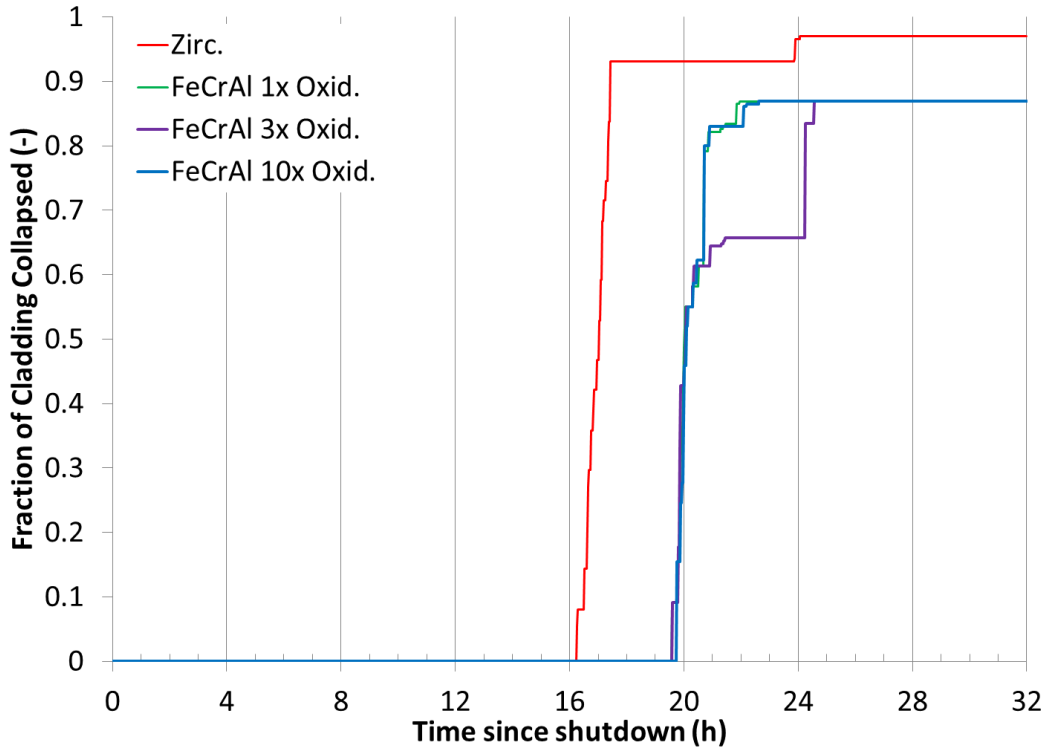
Figure 20. LTSBO–Fraction of cladding relocated.
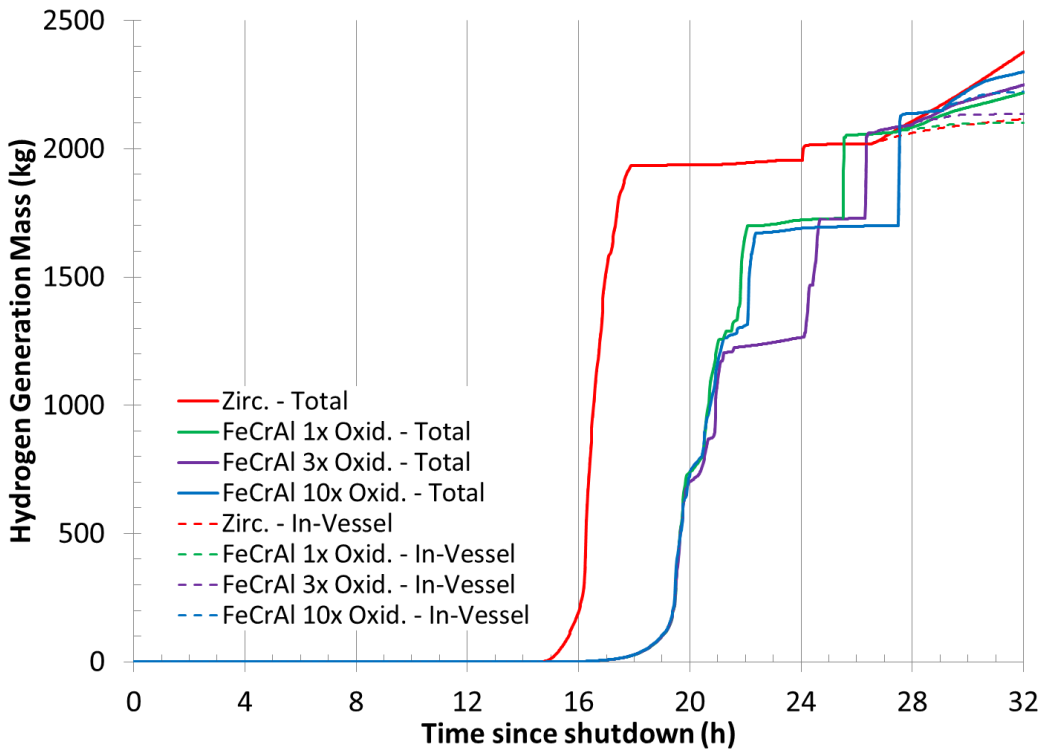
**Figure 21. LTSBO–Hydrogen generated in-vessel and total.**
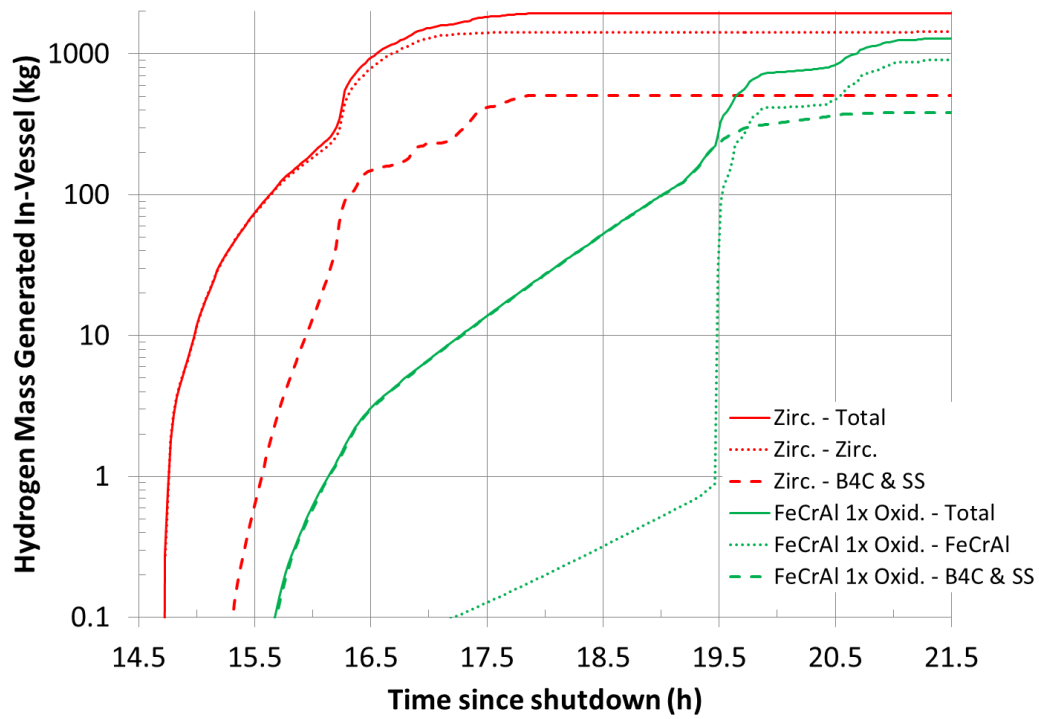
**Figure 22. LTSBO–Oxidation comparison between Zircaloy and FeCrAl 1× oxidation cases.**
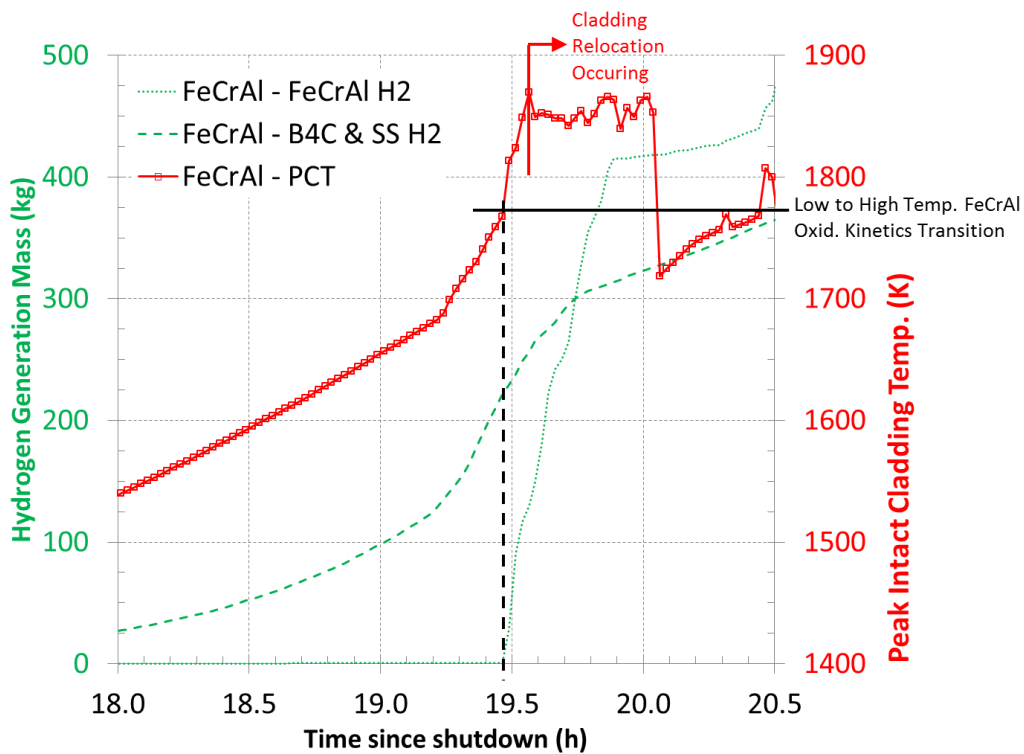
Figure 23. LTSBO–FeCrAl oxidation for FeCrAl 1× oxidation cases.
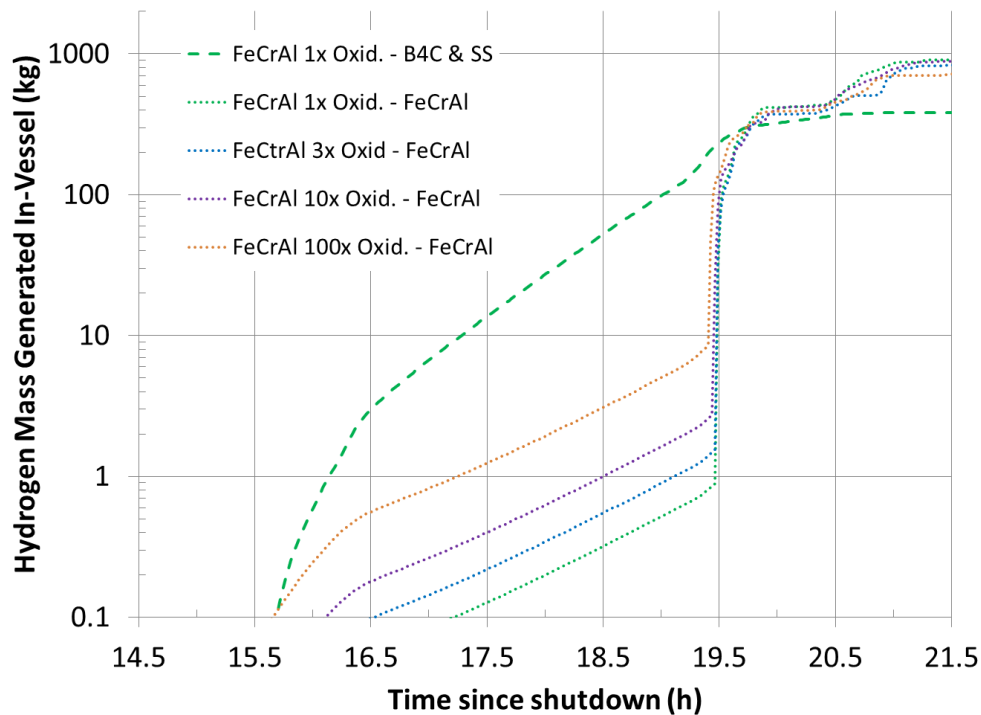
Figure 24. LTSBO–Comparison of FeCrAl oxidized.

4.3 SBO WITH MITIGATION LOSS AT 36 H

The figures of merit results for the cases are summarized in Table 16. Figure 25 through Figure 29 depict the reactor and containment pressure, RPV water level, peak intact cladding temperature, fraction of cladding collapsed, and the total and in-vessel hydrogen generation.

During this SBO, the operators have dc power for 36 h. As modeled, the operators depressurize the RPV at 2.9 h by manually actuating a SRV because of high temperatures in the suppression chamber. The RCIC is aligned to take suction from the suppression pool at 10.2 h because of the low water level of the condensate storage tank. The RCIC operates until 11.4 h when it is isolated because the suppression pool temperature exceeds the net positive suction head trip criterion. At 12 h, water injection starts by an external source through the feedwater line at 417 L/min (110 gpm). This water injection is maintained until the 36 h point.

At 36 h, dc power and external water injection are lost, the manually controlled SRV closes, and the RPV repressurizes up to the lowest automatic set point of the SRVs. As the RPV repressurizes, the water level briefly swells and then resumes boiling away. Eventually, the fuel become uncovered and begins to heat up. The Zircaloy cladding heats up faster than the FeCrAl cladding because of the oxidation kinetics. Despite its higher failure temperature, the Zircaloy cladding begins to relocate much sooner than the FeCrAl cladding. As modeled, operators do not take action to vent the containment. As such, containment slowly pressurizes over the accident progression and eventually fails because of the high pressure. Following fuel and containment failure, deflagrations are predicted to occur in the secondary containment building.

Interestingly, deflagrations are not predicted to occur in the FeCrAl 3× oxidation case. Also, the lower head fails much sooner for the FeCrAl 3× oxidation case compared with the FeCrAl 1× and 10× oxidation cases. While it was verified that this is what the code predicted, the causes for these discrepancies require further investigation. In general, it is noted that the accident simulations are indeed progressions that are heavily influenced by the earlier progression of the accident. Events and failure

33

modes are generally binary in that they either occur or do not occur. Furthermore, there are competing failure modes for areas such as the lower head and containment. These binary events can cause bifurcations in the accident progression among scenarios. Minor differences such as local material composition, temperature, location, etc., can result in actuating a binary failure mode or event.

The figures of merit (Table 16), show that when comparing the three FeCrAl cases to the base case Zircaloy system, the onset of hydrogen generation is delayed ~2 h for the FeCrAl cases. The timing to first release of the radionuclides in the gap is delayed by 0.5 h. The generation of substantial quantities of hydrogen (taken as 100 kg) is delayed by ~5.75 h. The timing to initial melting of the metallic cladding or collapse is delayed ~5 h. Following fuel failure, the difference between FeCrAl cases increases.

Comparing the base case Zircaloy system to that of the FeCrAl 1× or 10× oxidation cases, lower head failure is delayed 9.25–10 h. Containment failure is delayed ~2.5 h (containment is allowed to slowly pressurize without operator action). The first deflagration in the secondary containment building is delayed ~17 h. Less hydrogen and substantially less carbon monoxide is generated by the end of the simulation at 72 h.

Table 16. Figure of merit results for SBO with mitigation loss at 36 h

Figure of merit	Zircaloy	FeCrAl 1× Oxid.	FeCrAl 3× Oxid.	FeCrAl 10× Oxid.
0.5 kg of H_2 generated[a]	2,674	2,799	2,798	2,796
First fuel failure (gap release)[a]	2,685	2,712	2,711	2,712
100 kg of H_2 generated[a]	2,754	3,099	3,098	3,096
First cladding metal melting[a]	2,867	3,162	3,161	3,159
First cladding collapse[a]	2,868	3,171	3,170	3,168
Lower head failure[a]	3,274	3,878	3,469	3,829
Containment failure[a]	2,746	2,897	2,905	2,897
First deflagration in building[a]	2,876	3,919	NA[c]	3,882
0.5 kg noble gas release to environment[a]	2,748	2,904	2,913	2,906
H_2 gas generated at 72 h[b]	3,039	1,871	1,715	1,650
CO gas generated at 72 h[b]	17,285	5,563	6,145	5,051

[a]Measured in minutes.
[b]Measured in kilograms.
[c]NA=Not applicable (before end of simulation).
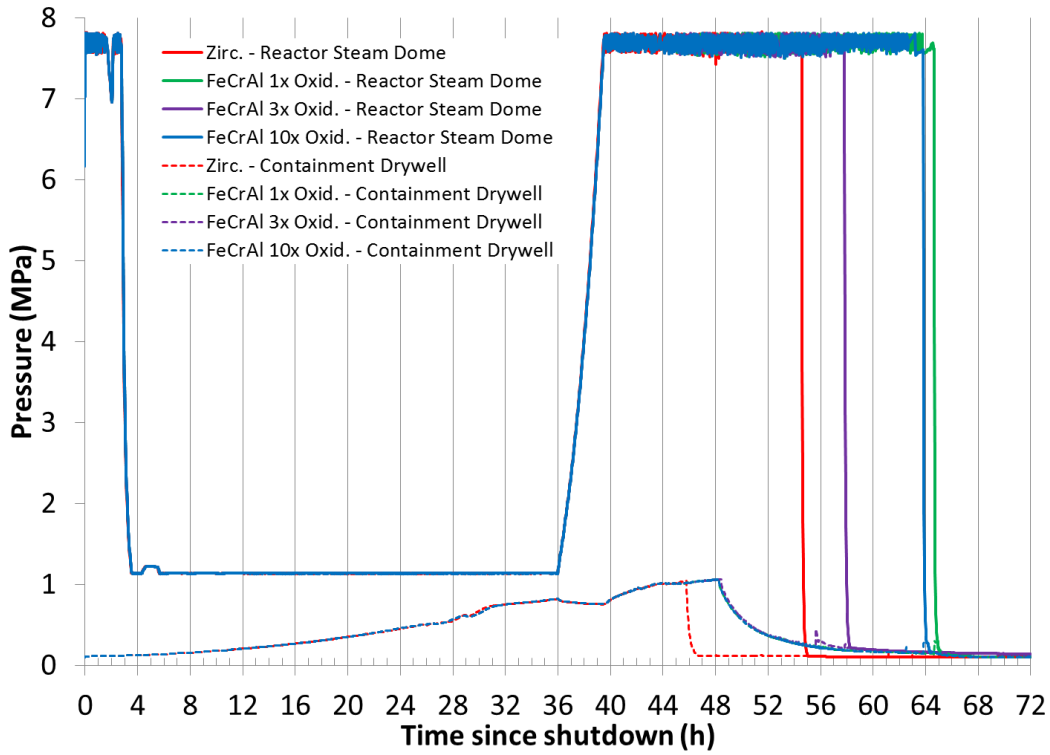
Figure 25. PMSBO–Reactor and containment pressure.
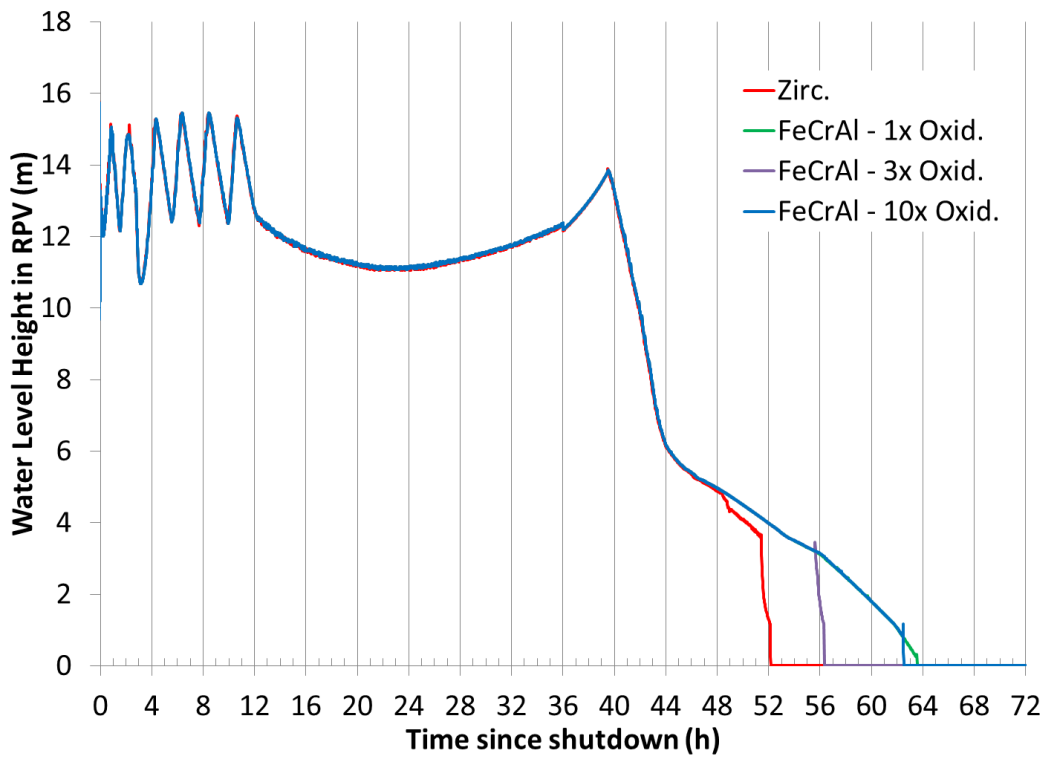
Figure 26. PMSBO–RPV water level.

35
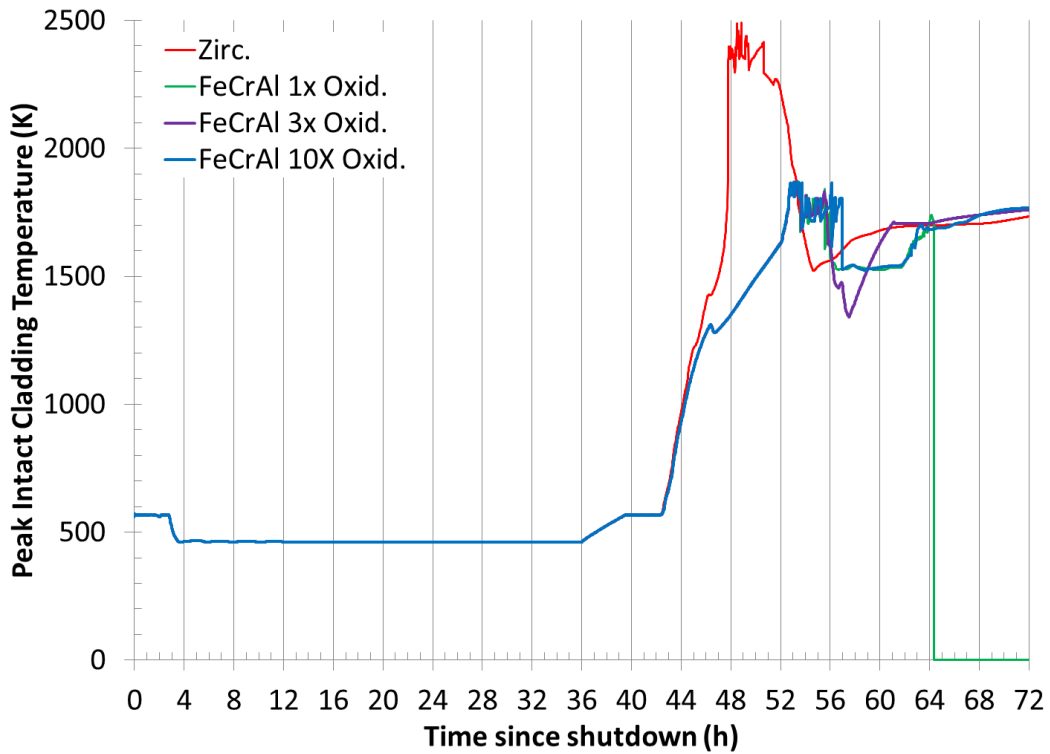
Figure 27. PMSBO–Peak intact cladding temperature.
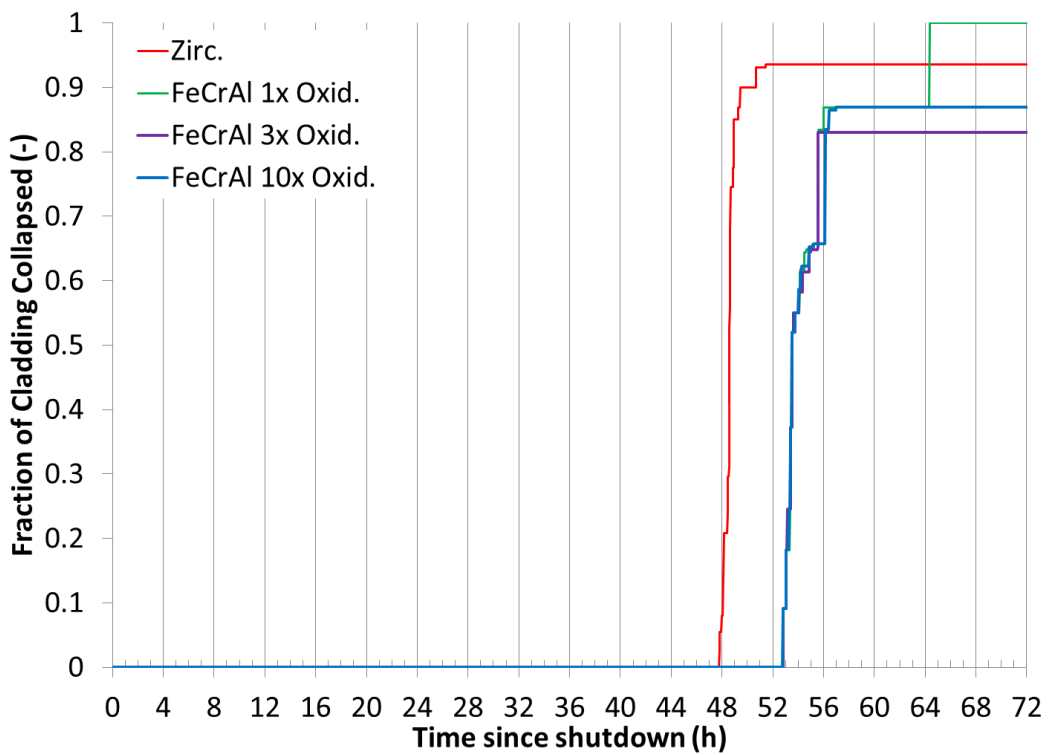
Figure 28. PMSBO–Fraction of cladding relocated.

36
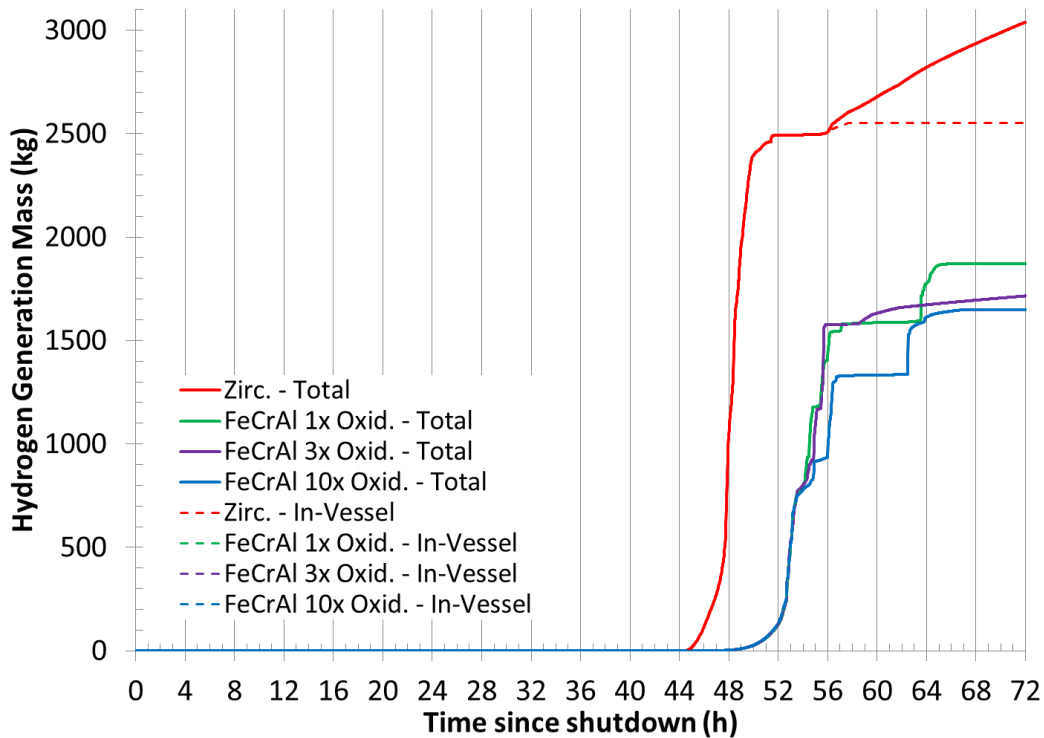
**Figure 29. PMSBO–Hydrogen generated in-vessel and total.**

4.4 MITIGATED STSBO

The figures of merit results for the cases are summarized in Table 17. Figure 30 through Figure 34 depict the reactor and containment pressure, RPV water level, peak intact cladding temperature, fraction of cladding collapsed, and the total and in-vessel hydrogen generation. Varying FeCrAl's low-temperature oxidation rate constant had negligible impact on the accident progression, and the results are similar to those predicted previously in Ref. [6].

During this STSBO, there are no operator actions or water injection initially by the RCIC, HPCI, or external means. Without operator actuation of the SRVs or the HPCI operating, the RPV remains pressurized. The water in the RPV boils away eventually uncovering the fuel. The fuel then begins to heat up and oxidize. At 2 h, water injection starts by an external source through the feedwater line at 568 L/min (150 gpm). This water injection is maintained throughout the rest of the simulation. The water injection is sufficient to reflood the core. For the Zircaloy case, the rapid oxidation results in heatup and collapse of much of the fuel. In contrast, no FeCrAl cladding is predicted to collapse during the simulation. For both cases, the core is reflooded and the accident is stabilized before lower head or containment failure.

The figures of merit (Table 17) show that when comparing the three FeCrAl cases to the base case Zircaloy system, the onset of hydrogen generation is delayed 37–39 min. The timing to first release of the radionuclides in the gap is delayed only 4 min. Only 91–94 kg of hydrogen are generated in the FeCrAl case, whereas 1,445 kg are generated by the Zircaloy case. No cladding melting or relocation is predicted to occur in any of the FeCrAl cases, in contrast to the Zircaloy case. For both simulations, negligible carbon monoxide is generated by 32 h as core debris does not leave the vessel to interact with the containment concrete.

Table 17. Figure of merit results for mitigated STSBO

Figure of merit	Zircaloy	FeCrAl 1× Oxid.	FeCrAl 3× Oxid.	FeCrAl 10× Oxid.
0.5 kg of H$_2$ generated[a]	70	109	108	107
First fuel failure (gap release)[a]	72	76	76	76
100 kg of H$_2$ generated[a]	97	NA[c]	NA	NA
First cladding metal melting[a]	112	NA	NA	NA
First cladding collapse[a]	112	NA	NA	NA
Lower head failure[a]	NA	NA	NA	NA
Containment failure[a]	NA	NA	NA	NA
First deflagration in building[a]	NA	NA	NA	NA
0.5 kg noble gas release to environment[a]	NA	NA	NA	NA
H$_2$ gas generated at 32 h[b]	1,445	91	91	94
CO gas generated at 32 h[b]	6	0	0	0

[a]Measured in minutes.
[b]Measured in kilograms.
[c]NA=Not applicable.
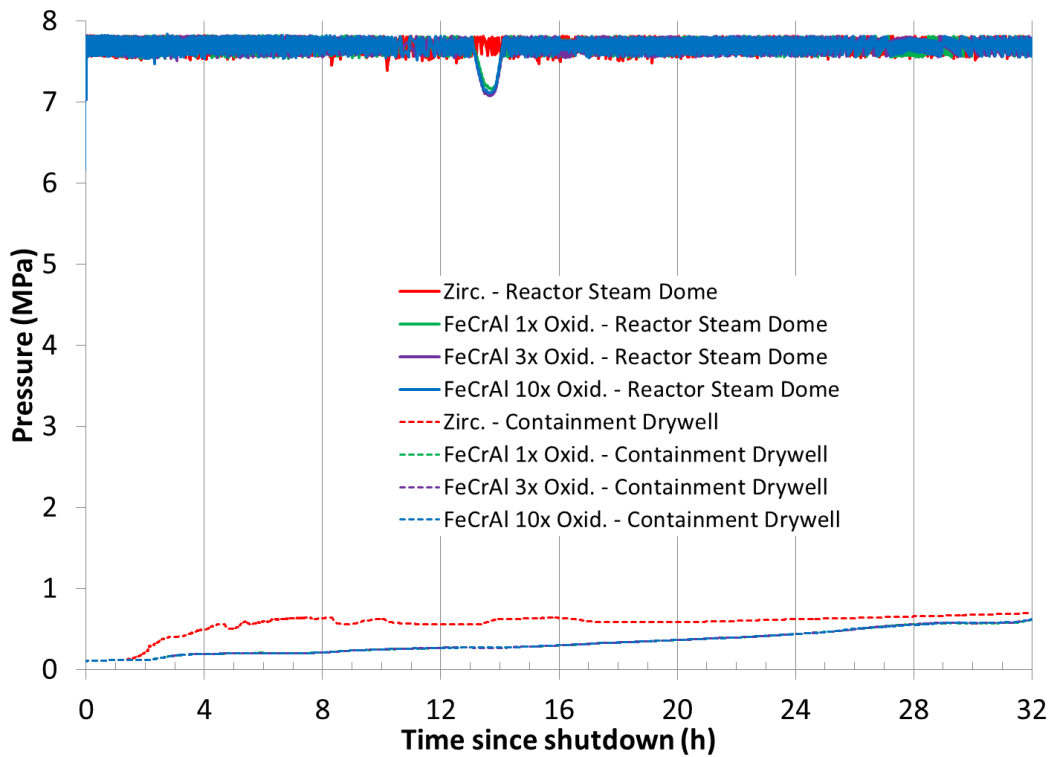
**Figure 30. MSTSBO–Reactor and containment pressure.**
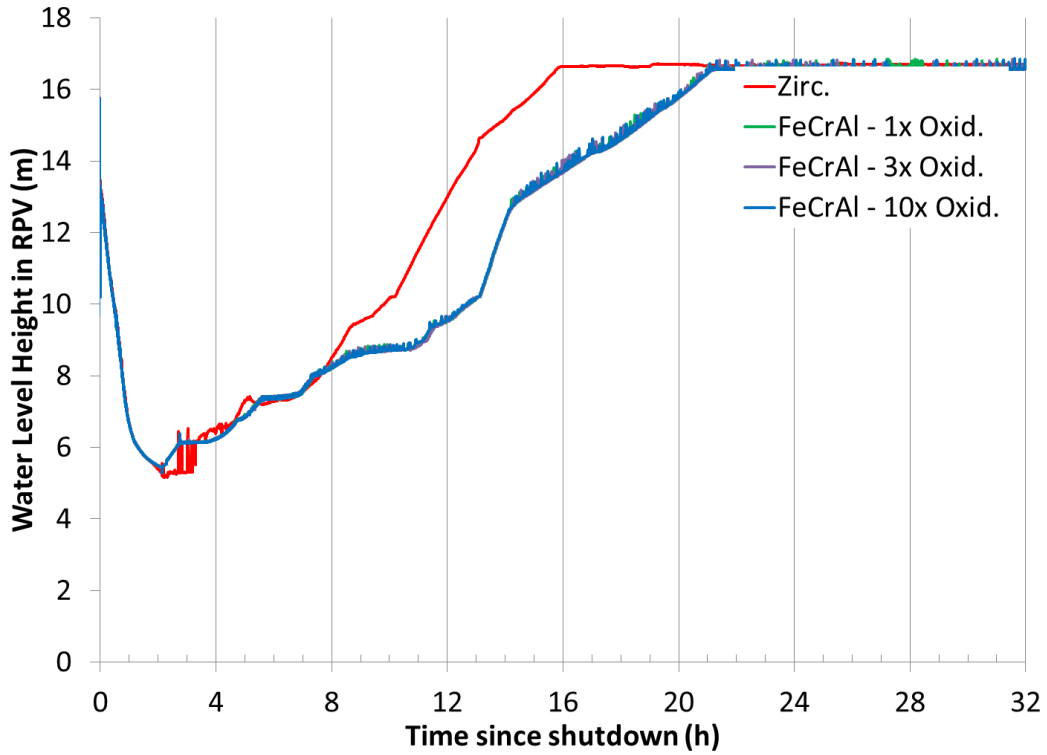
Figure 31. MSTSBO–RPV water level.
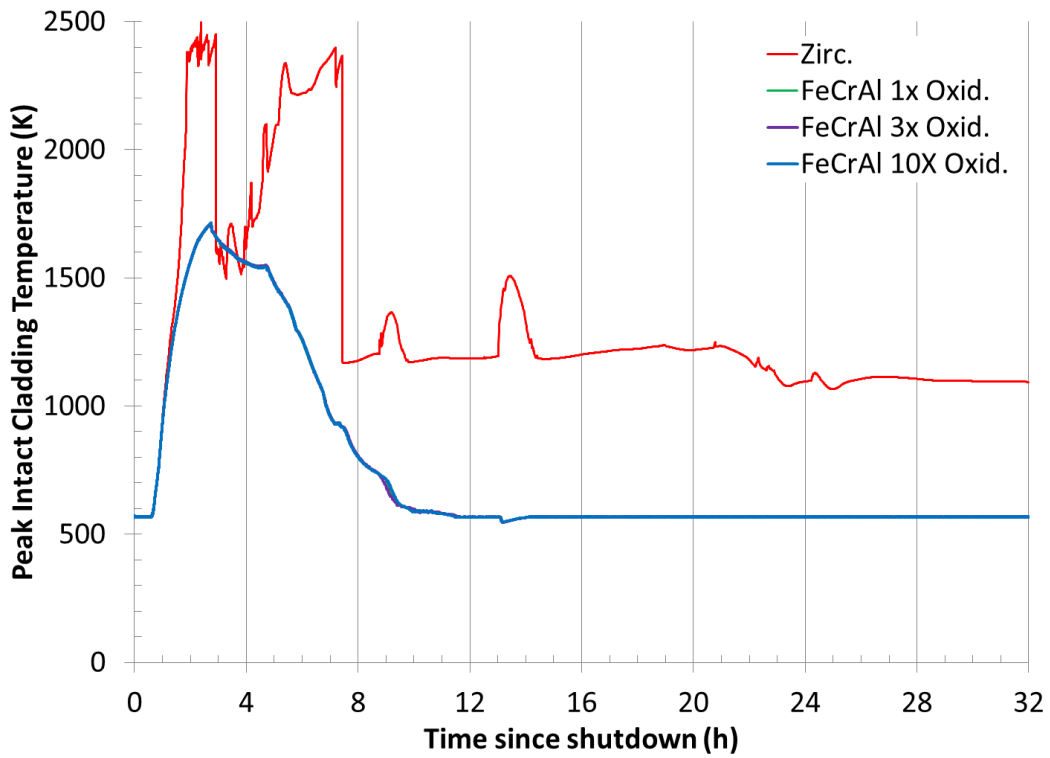
Figure 32. MSTSBO–Peak intact cladding temperature.
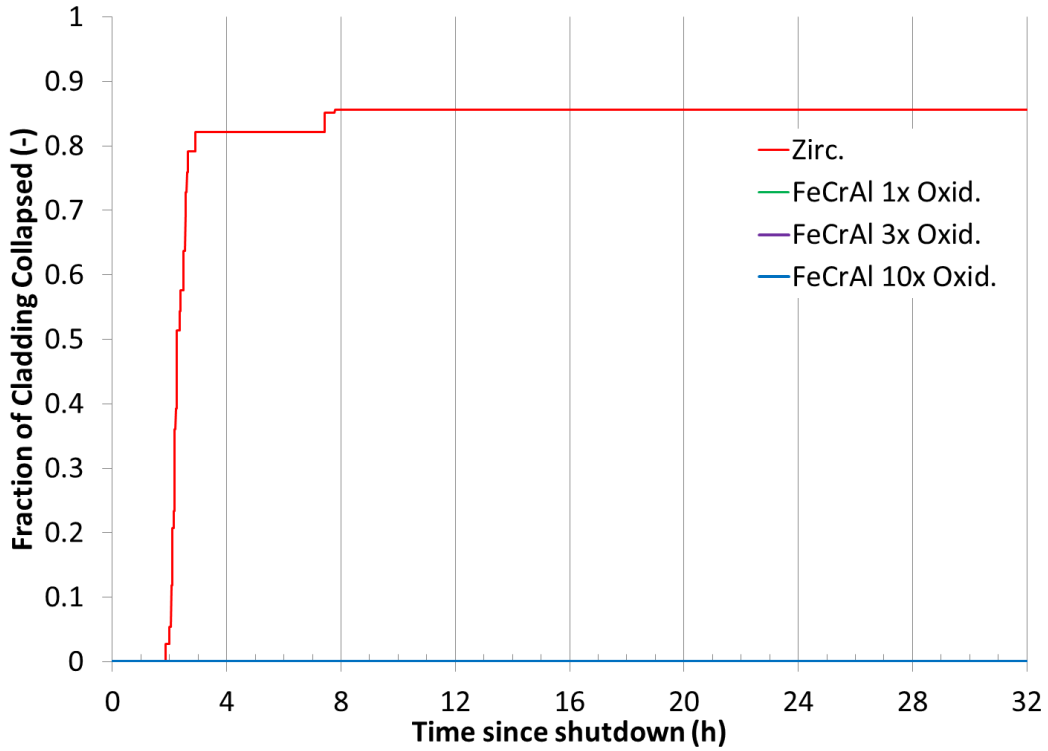
**Figure 33. MSTSBO–Fraction of cladding relocated.**
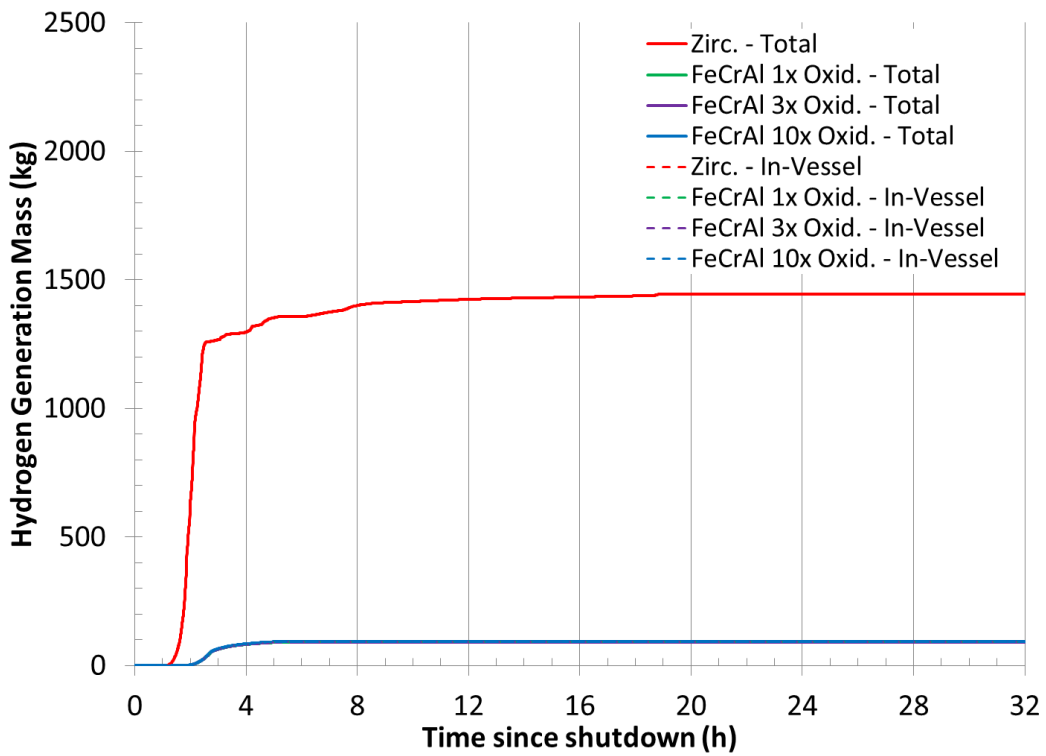
Figure 34. MSTSBO–Hydrogen generated in-vessel and total.

4.5 DISCUSSION OF RESULTS

Table 18 through Table 21summarize the difference in figures of merit between the FeCrAl cases and the Zircaloy case for the various scenarios. Values highlighted in green indicate an advantage with FeCrAl, red indicates a disadvantage with FeCrAl, and white indicates a neutral effect with FeCrAl. For the four accident scenarios simulated, parametrically varying the low-temperature oxidation rate constant by factors of 1, 3, and 10 that for APMT generally resulted in negligible changes in the early accident progression and minor changes in the accident progression after the fuel begins to relocate. As examined and discussed in Section 4.2, FeCrAl's low-temperature oxidation rate is so slow that the oxidation of FeCrAl is negligible and hydrogen production is dominated by the oxidation of the control blades. Increasing FeCrAl's low-temperature oxidation rate constant by a factor of 10 increases the amount of FeCrAl oxidized but still results in negligible oxidation relative to the control blades. After transitioning to the high-temperature oxidation kinetics, the oxidation of FeCrAl becomes a larger contributor to hydrogen production. In contrast, oxidation is dominated by the reaction of the Zircaloy in the traditional system that uses Zircaloy for the cladding and channel box.

The STSBO and MSTSBO accident scenarios were previously simulated [6]. As varying the low-temperature oxidation rate constant has only a minor impact, the results are similar to those previously obtained.

Table 18. STSBO figure of merit differences among Zircaloy and FeCrAl cases

Figure of merit	FeCrAl 1× Oxid.	FeCrAl 3× Oxid.	FeCrAl 10× Oxid.
0.5 kg of H_2 generated[a]	39	38	37
First fuel failure (gap release)[a]	4	4	4
100 kg of H_2 generated[a]	84	84	84
First cladding metal melting[a]	75	75	75
First cladding collapse[a]	79	79	79
Lower head failure[a]	-62	-53	-49
Containment failure[a]	-50	-29	-43
First deflagration in building[a]	-50	-29	-43
0.5 kg noble gas release to environment[a]	-39	-17	-32
H_2 gas generated by 16 h[b]	-299	-231	-443
CO gas generated by 16 h[b]	-4,800	-6,013	-4,710

[a]Measured in minutes.
[b]Measured in kilograms.

Table 19. LTSBO figure of merit differences among Zircaloy and FeCrAl cases

Figure of merit	FeCrAl 1× Oxid.	FeCrAl 3× Oxid.	FeCrAl 10× Oxid.
0.5 kg of H_2 generated[a]	73	73	71
First fuel failure (gap release)[a]	7	7	7
100 kg of H_2 generated[a]	202	202	200
First cladding metal melting[a]	195	195	194
First cladding collapse[a]	200	200	211
Lower head failure[a]	68	104	168
Containment failure[a]	133	180	208
First deflagration in building[a]	133	180	208
0.5 kg noble gas release to environment[a]	131	179	208
H_2 gas generated by 32 h[b]	-159	-128	-77
CO gas generated by 32 h[b]	-4,356	-4,595	-6,011

[a]Measured in minutes.
[b]Measured in kilograms.

Table 20. PMSBO figure of merit differences among Zircaloy and FeCrAl cases

Figure of merit	FeCrAl 1× Oxid.	FeCrAl 3× Oxid.	FeCrAl 10× Oxid.
0.5 kg of H_2 generated[a]	125	124	122
First fuel failure (gap release)[a]	27	26	27
100 kg of H_2 generated[a]	345	344	342
First cladding metal melting[a]	295	294	292
First cladding collapse[a]	303	302	300
Lower head failure[a]	604	195	555
Containment failure[a]	151	159	151
First deflagration in building[a]	1,043	[c]	1,006
0.5 kg noble gas release to environment[a]	156	165	158
H_2 gas generated by 72 h[b]	-1,168	-1,324	-1,389
CO gas generated by 72 h[b]	-11,722	-11,140	-12,234

[a]Measured in minutes.
[b]Measured in kilograms.
[c]FeCrAl cases predict this event does not occur during simulation.

Table 21. MSTSBO figure of merit differences among Zircaloy and FeCrAl cases

Figure of merit	FeCrAl 1× Oxid.	FeCrAl 3× Oxid.	FeCrAl 10× Oxid.
0.5 kg of H_2 generated[a]	39	38	37
First fuel failure (gap release)[a]	4	4	4
100 kg of H_2 generated[a]	[c]	[c]	[c]
First cladding metal melting[a]	[c]	[c]	[c]
First cladding collapse[a]	[c]	[c]	[c]
Lower head failure[a]	[d]	[d]	[d]
Containment failure[a]	[d]	[d]	[d]
First deflagration in building[a]	[d]	[d]	[d]
0.5 kg noble gas release to environment[a]	[d]	[d]	[d]
H_2 gas generated by 32 h[b]	-1354	-1354	-1351
CO gas generated by 32 h[b]	-6	-6	-6

[a]Measured in minutes.
[b]Measured in kilograms.
[c]FeCrAl cases predict this event does not occur during simulation.
[d]Both Zircaloy and FeCrAl cases predict this event does not occur during simulation.

As a result of the modifications of the model's HPCI and RCIC operation logic and operator actions for reactor depressurization (Section 3.4), the LTSBO simulations are much different from those obtained previously [6]. In the present LTSBO scenario, the RCIC was able to operate until 8 h when battery power is assumed to be lost. Thus, in the present LTSBO simulations, the RPV water level was successfully maintained and decay heat removed until the 8 h mark. In the previous LTSBO simulations, the RCIC and HPCI were isolated at 4.9 h because of low steam pressure. The accident was delayed further in the present LTSBO scenario. The gains afforded by the FeCrAl ATF concept are slightly higher than those obtained for the previous LTSBO simulations.

A PMSBO was simulated for which the RPV water level was maintained and decay heat removed until 36 h after scram. This is a longer duration than that previously simulated (loss of water injection at 16 and 24 h, [6]). At 36 h the decay heat is much lower and the boil down process much slower than in scenarios such as the STSBO and LTSBO. Because of the lower decay heat, the timing between the first cladding melting/collapse for the FeCrAl cases and that for the Zircaloy case was extended to ~5 h.

5.   SUMMARY

FeCrAl alloys are under active development as an ATF concept. The concept's key advantage over Zircaloy is its substantially slower oxidation kinetics up to 1,773 K (1,500°C). To support further development and future adoption, there is a need to assess the potential gains afforded by the FeCrAl ATF concept.

To assess the performance of the FeCrAl ATF concept under severe accident conditions, knowledge of a range of thermophysical and degradation characteristics is needed. Some properties, such as oxidation kinetics, can vary among FeCrAl alloys. The oxidation kinetics of the FeCrAl B136Y (Fe-13Cr-6Al wt %) alloy were investigated using the high-temperature furnace at ORNL. Fifteen segments of B136Y tubing were exposed to a flowing steam environment (~1 atm and 45–55 cm/s) while the system temperature was controlled.

In preparation for a planned QUENCH test using FeCrAl at KIT, one set of oxidation tests were conducted following the planned test temperature sequence. This includes holding the sample at 1,200°C for ~50 min. The test results indicate the B136Y cladding will remain intact for the anticipated peak temperatures of 1,375–1,400°C in the planned FeCrAl QUENCH test. For tests conducted to temperatures of 1,475°C and 1,500°C, the cladding suffered from extensive attack by the steam. In contrast, a second set of tests followed simplified temperature histories based on previously simulated SBO accident scenarios. The B136Y cladding, following more prototypic temperature histories, did not suffer from extensive attack during three tests conducted to 1,500°C.

Based on cladding sample surface area and pre- and posttest mass measurements, the amount of oxidation was determined for the tests. The parabolic oxidation kinetics for the APMT FeCrAl alloy underpredicted the amount of oxidation for the B136Y tubing for the samples not suffering from extensive attack. Although there was scatter in the data, increasing the APMT rate constant by a factor of 5 best reproduced the data set with respect to RMSD. The SBO tests conducted to 1,500°C were best reproduced by increasing the rate constant by a factor of 3.

To investigate the impact of the low-temperature oxidation kinetics (i.e., pre-breakaway oxidation), several SBO scenarios were simulated in which the rate constant was parametrically varied. Varying the rate constant by factors of 1, 3, and 10 resulted in negligible changes in the early accident progression and minor changes in the accident progression after the fuel began to relocate. When FeCrAl was employed for the cladding and channel box, the early hydrogen generation from the FeCrAl structures was very low and was instead dominated by the oxidation of the control blades. After exceeding the transition temperature to the high-temperature oxidation kinetics (i.e., post-breakaway oxidation) the FeCrAl material oxidized readily and became the dominate source of hydrogen. In contrast, for systems employing Zirconium-based alloys for the cladding and channel box, the oxidation of these materials dominates hydrogen production.

In general, the gains afforded by the FeCrAl ATF concept with respect to accident progression timing and flammable gas generation are consistent with previous efforts [6]. In the current study, water injection was lost at 0, 8, and 36 h into the accident for the STSBO, LTSBO, and PMSBO scenarios, respectively. Compared with the base case employing Zircaloy, the timing to the first melting/relocation of the fuel was delayed by 1.3, 3.3, and 5.0 h, respectively, when FeCrAl was employed. The additional coping time the FeCrAl ATF concept affords increases as the accident scenario is delayed. Gains in other metrics are summarized in Section 4.5.

Although a range of SBO severe accidents have been analyzed that are representative of higher probability severe accident scenarios [27] and the industry's experience with Fukushima Daiichi [28], there are many other possible severe accident scenarios. Other scenarios such as unmitigated loss of coolant accidents should be analyzed. The benefit of a delayed accident progression for operator actions (both on opportunity and success probability) or the lack of deflagrations influencing accident response was not accounted for in the analyses. Finally, assessments using other severe accident modeling tools, such as the MAAP code, should be pursued.

A need continues for additional information on the high-temperature degradation characteristics of FeCrAl cladding and channel boxes. Although a range of test data is available for Zircaloy fuel bundles [18], much accident behavior data is absent for FeCrAl. Tests such as those conducted at the QUENCH facility are needed. Additional needed information includes the possible eutectics formed during degradation, the failure points of the oxides under prototypic conditions, and the relocation characteristics of the collapsed fuel rods. In addition to in-vessel characteristics, further analysis is needed in the behavior of FeCrAl during the ex-vessel portion of the accident progression with respect to molten core-concrete interactions and the possibility for fuel-coolant interactions. Finally, a fuel assembly design has to be developed and analyzed that accounts for thermal-hydraulic, neutronic, fuel, and accident performance, as well as economic considerations.

Notwithstanding future work, the current analyses continue to suggest that the FeCrAl ATF concept would provide enhanced accident tolerance for a BWR during SBO severe accidents.

6. REFERENCES

1. F. Goldner, "Development Strategy for Advanced LWR Fuels with Enhanced Accident Tolerance," Enhanced Accident Tolerant LWR Fuels National Metrics Workshop, Germantown, MD, USA, October 2012.
2. K. A. Terrani, S. J. Zinkle, and L. L. Snead, "Advanced Oxidation Resistant Iron-Based Alloys for LWR Fuel Cladding," *J. Nuc. Mat.* 448(1–3), pp. 420–435 (2014).
3. B. A. Pint, K. A. Terrani, M. P. Brady, T. Cheng, and J. R. Keiser, "High temperature oxidation of fuel cladding candidate materials in steam-hydrogen environments," *J. Nuc. Mat.*, 440, pp.420–427 (2013).
4. K. A. Terrani, B. A. Pint, L. L. Snead, and Y. Yamamoto, "High-Temperature Steam Oxidation of Accident Tolerant Fuel Cladding Candidate materials," Proc. of a Technical Meeting Held at ORNL, IAEA-TECDOC-1797, USA, Oct 13–16, 2014.
5. J. Stuckert, M. Große, U. Stegmaier, and M. Steinbrück, *Results of Severe Fuel Damage Experiment QUENCH-15 with ZIRLOTM Cladding Tubes*, Karlsruhe Institute of Technology, KIT-SR 7576, 2011.
6. K. R. Robb, J. W. McMurray, and K. A. Terrani, *M2FT-16OR020205042: Severe Accident Analysis of BWR Core Fueled with UO2/FeCrAl with Updated Materials and Melt Properties from Experiments*, ORNL/TM-2016/237, Oak Ridge National Laboratory, Oak Ridge, TN, USA, June 2016.
7. Sandia National Laboratories, *MELCOR Computer Code Manuals*, Version 1.8.6, NUREG/CR-6119, Rev. 3, Sandia National Laboratories, Albuquerque, NM, USA, September 2005.
8. B. A. Pint, "Performance of FeCrAl for Accident-Tolerant Fuel Cladding in High Temperature Steam," *Corrosion Reviews*, 35 (2017).
9. L. J. Ott, K. R. Robb, and D. Wang, "Preliminary assessment of accident-tolerant fuels on LWR performance during normal operation and under DB and BDB accident conditions," *J. Nuc. Mat.*, 448(1–3), pp. 520–533 (2014).
10. K. R. Robb, "Analysis of the FeCrAl Accident Tolerant Fuel Concept Benefits During BWR Station Blackout Accidents," *Proc. of NURETH-16*, Chicago, IL, USA, August 30–September 4, 2015.
11. K. R. Robb, *Updated Peach Bottom Model for MELCOR 1.8.6: Description and Comparisons*, ORNL/TM-2014/207, Oak Ridge National Laboratory, Oak Ridge, TN, USA, September 2014.
12. A. B. Sandvik, "Kantahl APM (tube)" datasheet, updated August, 8, 2012, http://www.kanthal.com/en/products/material-datasheets/tube/kanthal-apm/, accessed 6/8/2016.
13. N. R. Brown, M. Todosow, and A. Cuadra, "Screening of advanced cladding materials and UN–U$_3$Si$_5$ fuel," *J. Nuc. Mat.*, 462, pp. 26–42 (2015).
14. J. J. Powers, N. M. George, A. Worrall, and K. A. Terrani, "Reactor Physics Assessment of Alternate Cladding Materials," *Transactions of the 2014 Water Reactor Fuel Performance Meeting / Top Fuel / LWR Fuel Performance Meeting* (WRFPM2014/TopFuel 2014), Sendai, Japan, September 14–17, 2014.
15. N. M. George, K. A. Terrani, J. J. Powers, A. Worrall, and G. I. Maldonado, "Neutronic Analysis of Candidate Accident-Tolerant Cladding Concepts in Pressurized Water Reactors," *Annals of N. E.* 75, pp. 703–712 (2015).
16. N. M. George, J. J. Powers, G. I. Maldonado, K. A. Terrani, and A. Worrall, "Neutronic Analysis of Candidate Accident-tolerant Cladding Concepts in Light Water Reactors," *Transactions of the American Nuclear Society*, 111 pp. 1363–1366 (2014).
17. N. M. George, J. J. Powers, G. I. Maldonado, A. Worrall, and K. A. Terrani, "Demonstration of a Full-core Reactivity Equivalence for FeCrAl Enhanced Accident Tolerant Fuel in BWRs," *Proc. of Advances in Nuclear Fuel Management V* (ANFM V), Hilton Head Island, SC, USA, March 29–April 1, 2015.

18. J. Rempe, M. Farmer, M. Corradini, L. Ott, R. Gauntt, and D. Powers, "Revisiting Insights from Three Mile Island Unit 2 Postaccident Examinations and Evaluations in View of the Fukushima Daiichi Accident," *J. Nuc. Sci. and Eng.* 172, pp. 223–248 (2012).

19. C. P. Massey, K. A. Terrani, S. N. Dryepondt, and B. A. Pint, "Cladding Burst Behavior of Fe-based Alloys Under LOCA," *J. Nuc. Mat.*, 470, pp 128–138 (2016).

20. J. W. McMurray et al., "Solid-liquid phase equilibria of Fe-Cr-Al alloys and spinels," *J. Nuc. Mat.*, 492, pp. 128–133 (2017).

21. S. V. Bechta et al., "Phase diagram of the UO_2–FeO_{1+x} system," *J. Nuc. Mat.*, 362, pp 46–52 (2007).

22. M. Barrachin, D. Gavillet, R. Dubourg, and A. De Bremaecker, "Fuel and fission product behaviour in early phases of a severe accident. Part I: Experimental results of the PHEBUS FPT2 test," *J. Nuc. Mat.*, 453, pp 340–354 (2014).

23. P. Pacenti et al., "Dissolution of UO_2 by FeO melts," *Corium Interaction and Thermochemistry, Interim Report*, European Commission Joint Research Centre, Environment Institute, EUR 18661 EN, 1998.

24. M. T. Farmer, L. Leibowitz, K. A. Terrani, and K. R. Robb, "Scoping Assessments of ATF Impact on Late Stage Accident Progression Including Molten Core-Concrete Interaction," J. *Nuc. Mat.*, 448(1–3), pp. 534–540 (2014).

25. Sandia National Laboratories, *MELCOR Computer Code Manuals*, Version 2.1, NUREG/CR-6119, Rev. 4, Sandia National Laboratories, Albuquerque, NM, USA, September 2008, Draft.

26. K. R. Robb, M. T. Farmer, and M. W. Francis, *Ex-Vessel Core Melt Modeling Comparison between MELTSPREAD-CORQUENCH and MELCOR 2.1*, ORNL/TM-2014/1, Oak Ridge National Laboratory, Oak Ridge, TN, USA, March 2014.

27. US Nuclear Regulatory Commission, *Severe accident risks: an assessment for five US nuclear power plants*, NUREG-1150, US Nuclear Regulatory Commission, Washington, DC, 1990.

28. Nuclear Emergency Response Headquarters, Government of Japan, *Report of Japanese Government to the IAEA Ministerial Conference on Nuclear Safety — The Accident at TEPCO's Fukushima Nuclear Power Stations*, June 2011.

APPENDIX A: B136Y OXIDATION TEST DATA

Table A-1. Oxidation test conditions summary

| Test | ID | Segment 1 | | | | Segment 2 | | | | Segment 3 | | | | Segment 4 |
		Temp. (°C)	Ramp Rate (°C/min)	Ramp Time (min)	Hold (min)	Temp. (°C)	Ramp Rate (°C/min)	Ramp Time (min)	Hold (min)	Temp. (°C)	Ramp Rate (°C/min)	Ramp Time (min)	Hold (min)	
1	B136Y312H1m.13615	600	20	30	1	1200	12.00	50	1	STOP				
2	B136Y312H50m.13634	600	20	30	1	1200	12.00	50	50.3	STOP				
3	B136Y314H1m.13650	600	20	30	1	1200	12.00	50	50.3	1400	11.1	18	1	STOP
4	B136Y315H1m.13655	600	20	30	1	1200	12.00	50	50.3	1500	11.1	27	1	STOP
7	B136Y324H1m.13615	600	20	30	1	1412	16.67	48.7	1	STOP				
8	B136Y325H1m.13694	600	20	30	1	1412	16.67	48.7	1	1500	4.17	21.1	1	STOP
9	B136Y322H1m.13695	600	20	30	1	1182	7.41	78.6	1	STOP				
10	B136Y325H1m.13696	600	20	30	1	1182	7.41	78.6	1	1500	1.81	175.5	1	STOP
11	B136Y321H1m.13697	600	20	30	1	1108	5.70	89.2	1	STOP				
12	B136Y325H1m.13709	600	20	30	1	1108	5.70	89.2	1	1500	1.57	249.4	1	STOP
15	B136Y3245H1m.13734	600	20	30	1	1200	12.00	50	50.3	1450	11.1	22.5	1	STOP
16	B136Y3247H1m.13742	600	20	30	1	1200	12.00	50	50.3	1475	11.1	24.8	1	STOP
17	B136Y3255H1m.13663	600	20	30	1	1182	7.41	78.6	1	1550	1.81	203.3	1	STOP
18	B136Y322H1min.13827	600	20	30	1	1200	12.00	50	150.9	STOP				
19	B136Y324H1min.13828	600	20	30	1	1200	12.00	50	50.3	1400	11.1	18	1	STOP

Table A-2. Oxidation test results summary

Test	ID	Dimensions			Initial Wt.	Final Wt.	Wt. Chg.	Area	SMG
		Outer Dia. (mm)	Length (mm)	Thickness (mm)	(mg)	(mg)	(mg)	(cm^2)	(mg/cm^2)
1	B136Y312H1m.13439	9.51	12.63	0.36	972.58	974.14	1.56	7.468	0.21
2	B136Y312H50m.13634	9.51	12.62	0.39	975.77	977.59	1.82	7.455	0.24
3	B136Y314H1m.13650	9.52	12.62	0.39	974.7	981.3	6.60	7.463	0.88
4	B136Y315H1m.13655	9.52	12.62	0.39	974.94	1439.62	464.68	7.463	62.26
7	B136Y324H1.13615	9.51	12.60	0.39	973.63	976.67	3.04	7.444	0.41
8	B136Y325H1m.13694	9.51	12.60	0.40	973.92	979.41	5.49	7.441	0.74
9	B136Y322H1m.13695	9.51	12.61	0.38	973.53	974.6	1.07	7.452	0.14
10	B136Y325H1m.13696	9.51	12.60	0.38	972.01	979.34	7.33	7.446	0.98
11	B136Y321H1m.13697	9.5	12.62	0.39	973.41	975.31	1.9	7.447	0.26
12	B136Y325H1m.13709	9.5	12.6	0.39	973.95	981.49	7.54	7.435	1.01
15	B136Y3245H1m.13734	9.51	12.61	0.39	975.25	979.26	4.01	7.449	0.54
16	B136Y3247H1m.13742	9.51	12.63	0.41	974.69	1416.97	442.28	7.456	59.32
17	B136Y3255H1m.13663	9.51	12.6	0.37	973.35	972.95	-0.4	7.448	-0.05
18	B136Y322H1min.13827	9.51	12.59	0.38	971.09	973.98	2.89	7.44	0.39
19	B136Y324H1min.13828	9.51	15.02	0.39	1155.21	1168.17	12.96	8.83	1.47